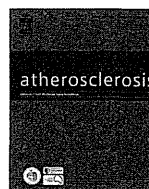




ELSEVIER

Contents lists available at ScienceDirect

## Atherosclerosis

journal homepage: [www.elsevier.com/locate/atherosclerosis](http://www.elsevier.com/locate/atherosclerosis)

## Three-dimensional multilayers of smooth muscle cells as a new experimental model for vascular elastic fiber formation studies

Ryo Ishiwata<sup>a</sup>, Utako Yokoyama<sup>a,\*</sup>, Michiya Matsusaki<sup>b</sup>, Yoshiya Asano<sup>c</sup>, Koji Kadowaki<sup>b</sup>, Yasuhiro Ichikawa<sup>a</sup>, Masanari Umemura<sup>a</sup>, Takayuki Fujita<sup>a</sup>, Susumu Minamisawa<sup>d</sup>, Hiroshi Shimoda<sup>c</sup>, Mitsuru Akashi<sup>b</sup>, Yoshihiro Ishikawa<sup>a,\*</sup><sup>a</sup> Cardiovascular Research Institute, Yokohama City University Graduate School of Medicine, 3-9 Fukuura, Kanazawa-ku, Yokohama, Kanagawa 236-0004, Japan<sup>b</sup> Department of Applied Chemistry, Graduate School of Engineering, Osaka University, Osaka, Japan<sup>c</sup> Department of Neuroanatomy, Cell Biology and Histology, Hirosaki University Graduate School of Medicine, Hirosaki, Japan<sup>d</sup> Department of Cell Physiology, Jikei University School of Medicine, Tokyo, Japan

## ARTICLE INFO

## Article history:

Received 9 August 2013

Received in revised form

20 January 2014

Accepted 21 January 2014

Available online 29 January 2014

## Keywords:

Blood vessels

Smooth muscle cells

Elastic fibers

Nanotechnology

Tissue engineering

Fibronectin

## ABSTRACT

**Objective:** Elastic fiber formation is disrupted with age and by health conditions including aneurysms and atherosclerosis. Despite considerable progress in the understanding of elastogenesis using the planar culture system and genetically modified animals, it remains difficult to restore elastic fibers in diseased vessels. To further study the molecular mechanisms, in vitro three-dimensional vascular constructs need to be established. We previously fabricated vascular smooth muscle cells (SMCs) into three-dimensional cellular multilayers (3DCMs) using a hierarchical cell manipulation technique, in which cells were coated with fibronectin–gelatin nanofilms to provide adhesive nano-scaffolds. Since fibronectin is known to assemble and activate elastic fiber-related molecules, we further optimized culture conditions.

**Methods and results:** Elastica stain, immunofluorescence, and electron microscopic analysis demonstrated that 3DCMs, which consisted of seven layers of neonatal rat aortic SMCs cultured in 1% fetal bovine serum (FBS) in Dulbecco's modified Eagle's medium, exhibited layered elastic fibers within seven days of being in a static culture condition. In contrast, the application of adult SMCs, 10% FBS,  $\epsilon$ -poly(L-lysine) as an alternative adhesive for fibronectin, or four-layered SMCs, failed to generate layered elastic fiber formation. Radioimmunoassay using [<sup>3</sup>H]valine further confirmed the greater amount of cross-linked elastic fibers in 3DCMs than in monolayered SMCs. Layered elastic fiber formation in 3DCMs was inhibited by the lysyl oxidase inhibitor  $\beta$ -aminopropionitrile, or prostaglandin E<sub>2</sub>. Furthermore, infiltration of THP-1-derived macrophages decreased the surrounding elastic fiber formation in 3DCMs. **Conclusion:** 3DCMs may offer a new experimental vascular model to explore pharmacological therapeutic strategies for disordered elastic fiber homeostasis.

© 2014 Elsevier Ireland Ltd. All rights reserved.

## 1. Introduction

Arterial walls have a highly organized layer structure that consists of various cells and extracellular matrix (ECM) components. In particular, the vascular media is composed of a dense population of concentrically organized smooth muscle cells (SMCs) and elastic fibers, and plays a pivotal role in maintaining sufficient blood

pressure, even during variations in hemodynamic stress. In physiological conditions, SMCs synthesize elastin and other specific molecules, which are incorporated into elastic fibers and arranged into concentric rings of elastic lamellae around the arterial media [1]. In contrast, arterial compliance and distensibility are impaired in the presence of cardiovascular disease and risk factors such as aortic aneurysm, atherosclerosis, ischemic heart disease, aging, hypertension, cigarette smoking, and diabetes [2]. Hence, impaired elastic properties are associated with arterial dysfunction and pathophysiology [2,3].

Changes in arterial elastic properties are the result of alterations in the intrinsic structural properties of the artery, including the fracturing and thinning of elastic fibers. Current approaches to

\* Corresponding authors. Tel.: +81 45 787 2575; fax: +81 45 787 1470.

E-mail addresses: [utako@yokohama-cu.ac.jp](mailto:utako@yokohama-cu.ac.jp), [CZL03430@nifty.com](mailto:CZL03430@nifty.com) (U. Yokoyama), [yishikaw@med.yokohama-cu.ac.jp](mailto:yishikaw@med.yokohama-cu.ac.jp) (Y. Ishikawa).

examining the elastogenesis and degradation of elastic fibers rely heavily on the use of the planar culture of vascular SMCs and genetically modified animals. These approaches have been instrumental in numerous discoveries and have been modified to create very elegant experimental designs [1,4–7]. Currently, however, no pharmacological strategy to promote elastogenesis and prevent the degradation of elastic fiber formation is available, and the molecular mechanisms of the regulation of elastic fiber formation remain to be studied. The two-dimensional (2D) monolayer culture system is a useful method for isolating specific factors and their effects on specific cell types [5–7], but it lacks the native-like layered structure of elastic fibers. Therefore, changes in the spatial arrangement of elastic fibers induced by various stimuli and the infiltration of immune cells cannot be observed. In-vivo analysis, on the other hand, often fails to discriminate among the various and complex factors. In this context, in vitro reconstruction vessel models overcoming these limitations are considered potential platforms of vascular biology that can provide further insights into the spatio-temporal molecular mechanisms of elastic fiber formation.

We previously developed a novel three-dimensional (3D) cell construction method [8] and created 3D-layered blood vessel constructs consisting of human umbilical arterial SMCs and human umbilical vascular endothelial cells [9]. To develop the 3D-cellular multilayers (3DCMs), we fabricated nanometer-sized cell adhesives like ECM scaffolds onto the surface of a cell membrane, which enables another cellular layer to adhere to the coated cell surface. We employed a layer-by-layer (LbL) technique to fabricate fibronectin–gelatin nanofilms onto living cell membranes, because the LbL technique produces nanometer-sized polymer films with a controllable nanometer thickness through the alternate immersion into interactive polymer solutions. We found that approximately 6 nm of fibronectin-based nanofilms were suitable for developing stable adhesive scaffolds and for creating allogeneic or xenogeneic multiple cell layers.

In addition to the cell adhesion effect, fibronectin has been known to orchestrate the assembly of the ECM [10–15]. In particular, recent reports suggest that fibronectin fiber assembles pericellularly into fibrillin microfibrils that have a complex structural organization and are widespread in elastic tissues [10,16]. Furthermore, fibronectin binds to lysyl oxidase (LOX), a cross-linking enzyme for elastic fibers, and acts as a scaffold for enzymatically active 30 kDa LOX [14]. Using scanning electron microscopy and transmission electron microscopy, we observed that fibronectin formed extracellular fibrils in the abovementioned 3DCMs within 24 h cultures [9], suggesting that fibronectin-coated SMCs have the potential to produce elastic fiber assemblies. In this context, we aimed to create the first scaffold-free 3D cellular multilayers (3DCMs) that are specifically designed for investigating the spatial regulation of vascular elastic fibers by employing this LbL assembly technique. The present study demonstrates that the optimized culture conditions provided layered elastic fiber formation in the 3DCMs consisting of neonatal rat SMCs within seven days of static culture conditions. In the 3DCMs, it was observed in the vertical view that macrophage infiltration or prostaglandin E<sub>2</sub> (PGE<sub>2</sub>) changed the spatial arrangement of elastic fibers.

## 2. Materials and methods

Expanded materials and methods are described in Supplemental data.

### 2.1. Animals

Neonate (day 1) and adult Wistar rats (4–5 months old) were obtained from Japan SLC, Inc. (Shizuoka, Japan). All animal studies

were approved by the institutional animal care and use committees of Yokohama City University.

### 2.2. Cell culture

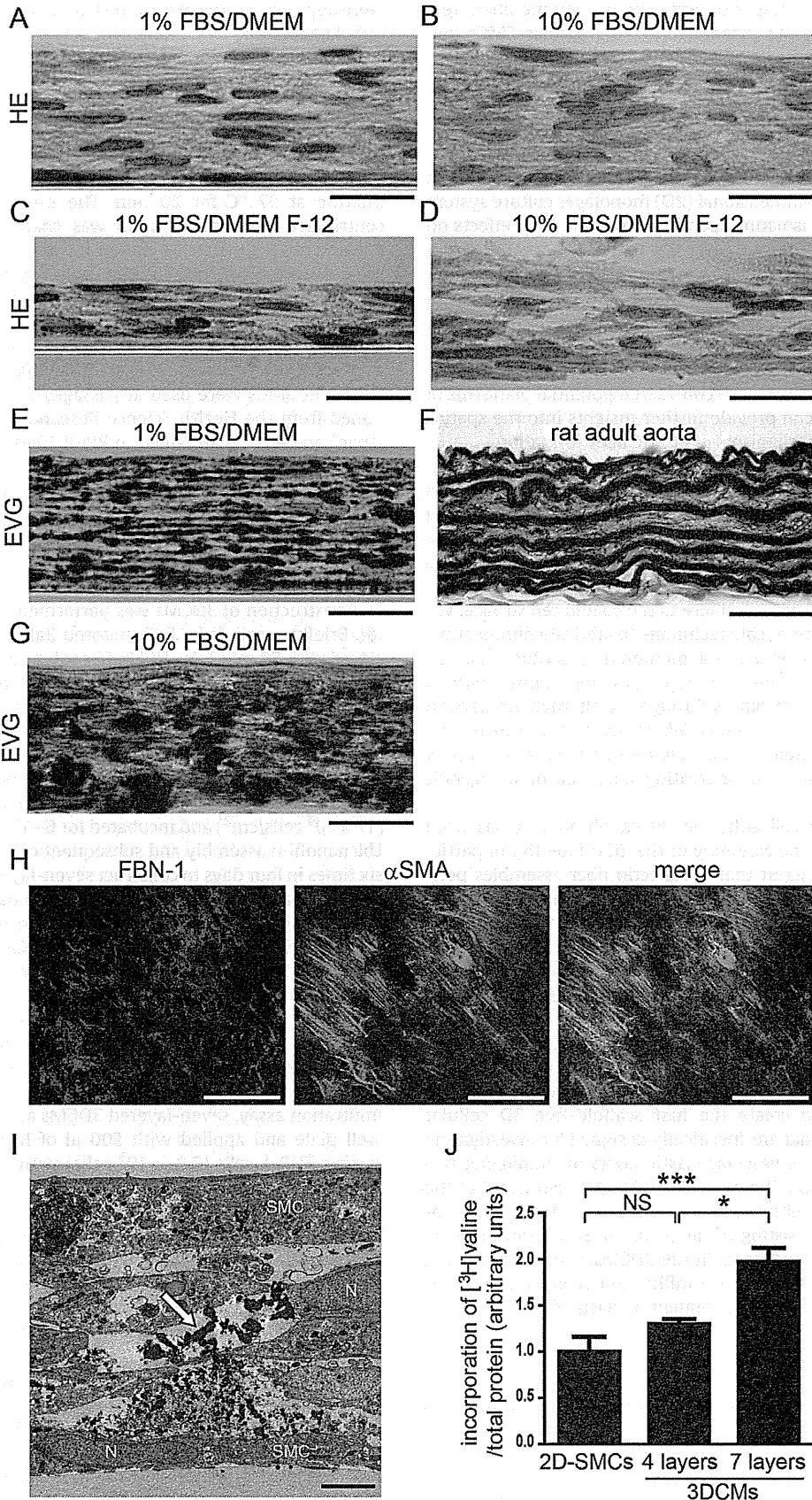
Vascular SMCs in primary culture were obtained from the aorta of rat neonates (day 1) as previously described [17–19]. Briefly, the minced tissues were digested with a collagenase-dispase enzyme mixture at 37 °C for 20 min. The cell suspensions were then centrifuged, and the medium was changed to a collagenase II enzyme mixture. After 12 min of incubation at 37 °C, cell suspensions were plated on 35 mm poly-L-lysine-coated dishes. The growth medium contained Dulbecco's modified Eagle medium (DMEM) with 10% fetal bovine serum (FBS), 100 U/ml penicillin, and 100 mg/ml streptomycin (Invitrogen, Carlsbad, CA). Human adult aortic SMCs were obtained from Lonza (Walkersville, MD, USA). The confluent SMCs were used at passages 5–7. THP-1 cells were obtained from the Health Science Research Resources Bank (Osaka, Japan) and were maintained in RPMI 1640 medium (Wako, Osaka, Japan) supplemented with 10% FBS. All cells were cultured in a moist tissue culture incubator at 37 °C in 5% CO<sub>2</sub>–95% ambient mixed air.

### 2.3. Construction of 3DCMs

Construction of 3DCMs was performed as previously described [8]. Briefly, a cell disk LF (Sumitomo Bakelite, Tochigi, Japan) was rinsed with 50 mM Tris–HCl buffer solution (pH 7.4) for 15 min and coated with fibronectin (0.2 mg/ml) for 30 min at 37 °C. SMCs were cultured on the cell disk ( $11 \times 10^4$  cells/cm<sup>2</sup>) and incubated for 12 h in 10% FBS/DMEM. The monolayered SMCs were then immersed alternatively in a solution of fibronectin (0.2 mg/ml) and gelatin (0.2 mg/ml). After nine steps of LbL assembly with fibronectin and gelatin, a second cell layer was seeded on the first cell layer ( $11 \times 10^4$  cells/cm<sup>2</sup>) and incubated for 6–12 h at 37 °C. The cycles of LbL nanofilm assembly and subsequent cell seeding were repeated six times in four days to construct seven-layered 3DCMs. During the first four days, the medium was refreshed daily. Twelve hours after the seeding of the last layer, the culture media was changed to DMEM or DMEM/F-12 (Gibco, Carlsbad, CA) containing 1% FBS or 10% FBS. The 3DCMs were incubated for an additional 48 h and either fixed in buffered 10% formalin or harvested in TRIzol (Invitrogen, Carlsbad, CA). The time-course of the 3DCM experiments is shown in Supplemental Fig. 1A. Stimulation by  $\beta$ -amino-propionitrile (BAPN) or PGE<sub>2</sub> (1  $\mu$ M) was performed simultaneously with the medium change on day 5. For macrophage infiltration assay, seven-layered 3DCMs at day 5 were put on a 24-well plate and applied with 500  $\mu$ l of RPMI 1640 medium containing THP-1 cells ( $2.0 \times 10^5$  cells) with or without phorbol 12-myristate 13-acetate (PMA, 0.1  $\mu$ M). The 3DCMs were incubated for 1 h at 37 °C. Next, unattached THP-1 cells were washed out with PBS and 3DCMs were incubated in 1% FBS/DMEM for 72 h until fixation. Control monolayered neonatal rat aortic SMCs (2D-SMCs) were plated on day 4 in the same density as a single layer in 3DCMs ( $11 \times 10^4$  cells/cm<sup>2</sup>), and were incubated for 48 h. Four-layered 3DCMs were constructed from day 3 following the same time-course. The proportional increase in the thickness of 3DCMs with the number of seeding events was shown in Supplemental Fig. 1B. To confirm the effect of fibronectin nanofilms,  $\epsilon$ -poly(lysine) (0.2 mg/ml) was used as an alternative adhesive polymer.

### 2.4. Quantitative measurement of insoluble elastin

Newly synthesized insoluble elastin was measured as previously described [20,21]. Briefly, after the seven-layered 3DCMs and 2D-



SMCs were constructed for four days and one day, respectively, as mentioned above, they were incubated in 2 ml of 1% FBS/DMEM in the presence of 5  $\mu\text{Ci}$  [ $^3\text{H}$ ]valine (ART 0466, American Radiolabeled Chemicals, Inc., St. Louis, MO) for an additional three days. One day after the monolayered SMCs were plated, the cells were harvested in 0.1 M acetic acid on ice. After centrifugation, the pellets were boiled in 0.1 N NaOH for 1 h. The NaOH-insoluble fractions were collected by centrifugation and were boiled in 5.7 N HCl for 1 h. The samples mixed with scintillation fluid were measured for radioactivity using a scintillation counter (Beckman Coulter).

### 2.5. Statistical analyses

Data are presented as the mean  $\pm$  standard error of the mean (SEM) of independent experiments. Data were analyzed by the unpaired Student's *t*-test or one-way analysis of variance (ANOVA) followed by Newman–Keuls multiple comparison test.  $p < 0.05$  was considered significant.

## 3. Results

### 3.1. 3DCMs exhibited layered elastic fiber formation

Most of the elastic fiber proteins are expressed in the second half of development and increase throughout the early postnatal period [22]. This is followed by a decrease in expression to low levels that persist through adulthood [23]. Consistent with this *in vivo* evidence, it has been suggested that neonatal rat SMCs produce a greater amount of elastin and elastic fibers compared to adult rat SMCs [24,25]. We confirmed that mRNA expression levels of elastic fiber-related genes, such as tropoelastin, fibrillin-1, fibulin-4, fibulin-5, LOX, and LOX-like 1, are significantly greater in the neonatal rat aorta (1 day old) than in the adult rat aorta (Supplemental Fig. 2).

On the basis of these data, we used neonatal rat SMCs to fabricate 3DCMs as *in vitro* vascular constructs. First, we cultured 3DCMs with four different culture media, including DMEM and DMEM F-12, because DMEM F-12 includes proline, one of the major amino acids that constitutes elastin protein, and copper, which enhances LOX activity [26]. Contrary to expectations, nucleus counting using HE stain revealed that viability was better in the 3DCMs cultured in DMEM (Fig. 1A–B, Supplemental Fig. 3) than in DMEM F-12 containing either 10% or 1% FBS (Fig. 1C–D). Next, we compared elastic fiber formation using Elastica van Gieson (EVG) stain in 3DCMs cultured in DMEM containing 10% or 1% FBS. We found that 3DCMs cultured in 1% FBS/DMEM exhibited layered elastic fiber formation (Fig. 1E), although the elastic fiber formation did not reach that observed in adult rat aorta (Fig. 1F). The 3DCMs culture in 10% FBS/DMEM exhibited a certain amount of positive stain of elastic fibers, but no layered elastic fiber formation was clearly detected (Fig. 1G). In the 3DCMs culture in 1% FBS/DMEM, co-immunofluorescence for fibrillin-1 and  $\alpha$ -smooth muscle actin ( $\alpha$ SMA) demonstrated a fiber meshwork of fibrillin-1 on the SMC surface (Fig. 1H). Electron microscopic analysis also confirmed the presence of elastic laminae between SMC layers (Fig. 1I).

To investigate whether the use of fibronectin nanofilms is required for elastic fiber formation in the 3DCMs, we applied

$\epsilon$ -poly(lysine), a synthesized polymer that electrically binds to gelatin, as an alternative to fibronectin in the 3DCMs. We found that  $\epsilon$ -poly(lysine) did not provide layered elastic fiber formation (Supplemental Fig. 4A). As expected, the 3DCMs composed of adult human aortic SMCs or adult rat aortic SMCs also did not exhibit elastic fiber formation (Supplemental Fig. 4B–C). Furthermore, we compared elastic fiber formation between the 3DCMs and another 3D model, i.e., the spheroid culture system. We constructed spheroids of neonatal rat SMCs with the same culture conditions of 3DCM construction (Supplemental Fig. 5A) and found that a few elastic laminae were formed in the outer shell of rat SMC spheroids, but not in the porous core (Supplemental Fig. 5B–C).

To quantify the amount of mature (i.e., cross-linked) elastic fibers in 3DCMs, we metabolically labeled newly synthesized elastin with [ $^3\text{H}$ ]valine, and measured the incorporation of [ $^3\text{H}$ ]valine in the NaOH-insoluble fraction of these cells, which reflects the amount of newly synthesized mature elastic fibers [27]. As shown in Fig. 1J, in 3DCMs cultured with 1% FBS/DMEM, we detected a significant increase in the incorporation of [ $^3\text{H}$ ]valine into the insoluble fraction compared to 2D-SMCs cultured in the same culture medium. Interestingly, seven-layered 3DCMs produced a larger amount of cross-linked elastic fibers than four-layered 3DCMs even if the values were compared in the same amount of protein (Fig. 1J and Supplemental Fig. 4D). These data suggest that seven-layered 3DCMs consisting of fibronectin coating neonatal rat aortic SMCs cultured in 1% FBS/DMEM produced layered elastic fibers *in vitro*.

### 3.2. Expression of elastic fiber-related genes in 3DCMs

Elastic fibers are complex structures that contain elastin as well as microfibrils and fibulins [1]. Elastin is the major component of mature elastic fibers, and microfibrils, such as fibrillin-1 and fibrillin-2, are known to facilitate elastin assembly and provide overall structure to the growing elastic fiber [1]. Tropoelastin's lysine residues are, in turn, modified to form covalent cross-links between and within elastin molecules by LOX, resulting in the functional form of elastic fibers [1,26]. The deposition of fibulin-5 on microfibrils also promotes the coacervation and alignment of tropoelastins on microfibrils, and facilitates the cross-linking of tropoelastin by tethering LOX-like 1, 2, and 4 enzymes [20]. Fibulin-4 interacts with LOX and recruits LOX to elastin monomers as well [28].

We examined the mRNA expression levels of these genes in the 3DCMs cultured in DMEM containing 1% or 10% FBS and 2D-SMCs. The expression levels of tropoelastin and fibrillin-2 mRNAs were greater in the 3DCMs cultured in 1% FBS/DMEM than in 10% FBS/DMEM (Fig. 2A–B). The expression levels of other genes, including fibrillin-1, fibulin-4, fibulin-5, LOX, and LOX-like 1, were similar among different serum concentrations (Fig. 2C–G). Similar serum withdrawal effects on tropoelastin and fibrillin-2 mRNA were also observed in 2D-SMCs (Supplemental Fig. 6A–B). In 3DCMs cultured in 1% FBS/DMEM, abundant protein expressions of tropoelastin and LOX were also observed (Fig. 2H–I). However, there was no difference in the expression of elastic fiber-related genes between 2D-SMCs and 3DCMs (Fig. 2A–G, J–K). These data

**Fig. 1.** 3DCMs cultured in 1% FBS/DMEM exhibited layered elastic fibers. (A–B) Hematoxylin eosin (HE) stain of 3DCMs cultured in DMEM containing either 1% (A) or 10% FBS (B). HE stain of 3DCMs cultured in DMEM F-12 containing either 1% (C) or 10% FBS (D). (E) Elastica van Gieson (EVG) stain of 3DCMs cultured in 1% FBS/DMEM. Scale bars: 10  $\mu\text{m}$ . (F) EVG stain of rat adult aorta. Scale bar: 50  $\mu\text{m}$ . (G) EVG stain of 3DCMs cultured in 10% FBS/DMEM. Scale bar: 10  $\mu\text{m}$ . (H) Confocal images of the fibrillin-1 and  $\alpha$ SMA immunofluorescence in the 3DCMs cultured in 1% FBS/DMEM. red: fibrillin-1. Green:  $\alpha$ SMA. Scale bar: 50  $\mu\text{m}$ . (I) Electron microscopic image of 3DCMs. White arrow indicates elastic fibers. N: nucleus. Scale bar: 2.0  $\mu\text{m}$ . (J) Radioimmunoassay of elastogenesis in 2D-SMCs, four-layered 3DCMs, and seven-layered 3DCMs cultured in 1% FBS/DMEM.  $n = 4–8$ . \* $p < 0.05$ ; \*\*\* $p < 0.001$ ; NS: not significant.

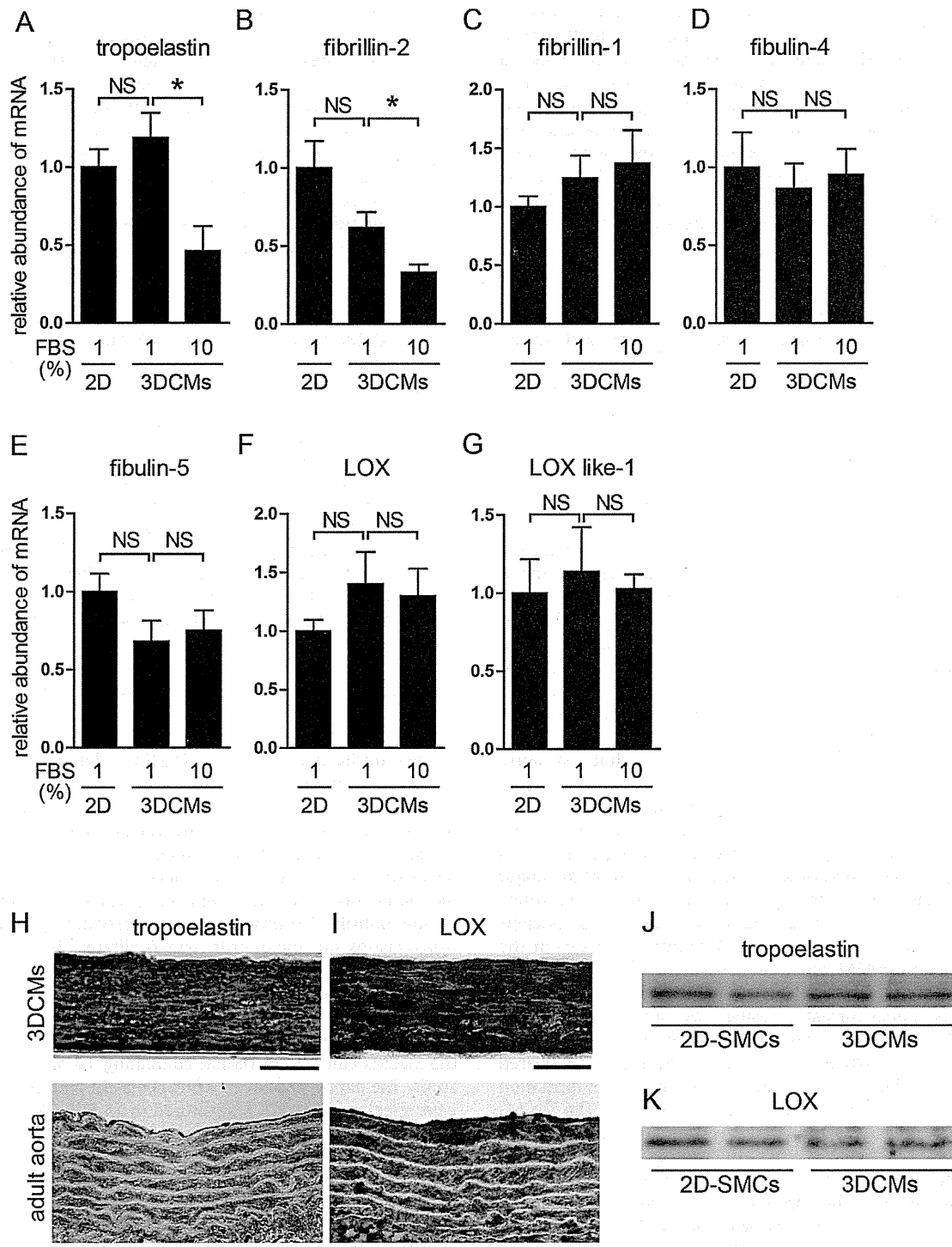


**Fig. 2.** Expressions of elastic fiber-related genes in 3DCMs. (A–G) Expressions of tropoelastin (A), fibrillin-2 (B), fibrillin-1 (C), fibulin-4 (D), fibulin-5 (E), LOX (F), and LOX-like 1 (G) mRNA were compared between 2D-SMCs (2D) cultured in 1% FBS/DMEM and 3DCMs cultured either in 1% FBS/DMEM or 10% FBS/DMEM.  $n = 6–8$ . \* $p < 0.05$ . NS: not significant. (H–I) Immunohistochemistry for tropoelastin (H) and LOX (I). Brown color indicates positive staining, top panels: 3DCMs. Scale bars: 10  $\mu$ m lower panels: rat adult aorta. Scale bars: 50  $\mu$ m. (J–K) Immunoblot analysis for elastin (J), and LOX (K) in 2D-SMCs and 3DCMs.

suggest that the 3D-SMC arrangement per se did not affect elastic fiber-related gene expressions, and that the serum withdrawal likely induced an enhancement of the expression of tropoelastin and fibrillin-2, resulting in elastic fiber formation in the 3DCMs cultured in 1% FBS/DMEM.

### 3.3. Characterization of the SMC phenotype in 3DCMs

In contrast to the highly differentiated SMCs in mature adult organs, SMCs readily undergo phenotypic changes after isolation and subsequent conventional planar culture [29]. We examined

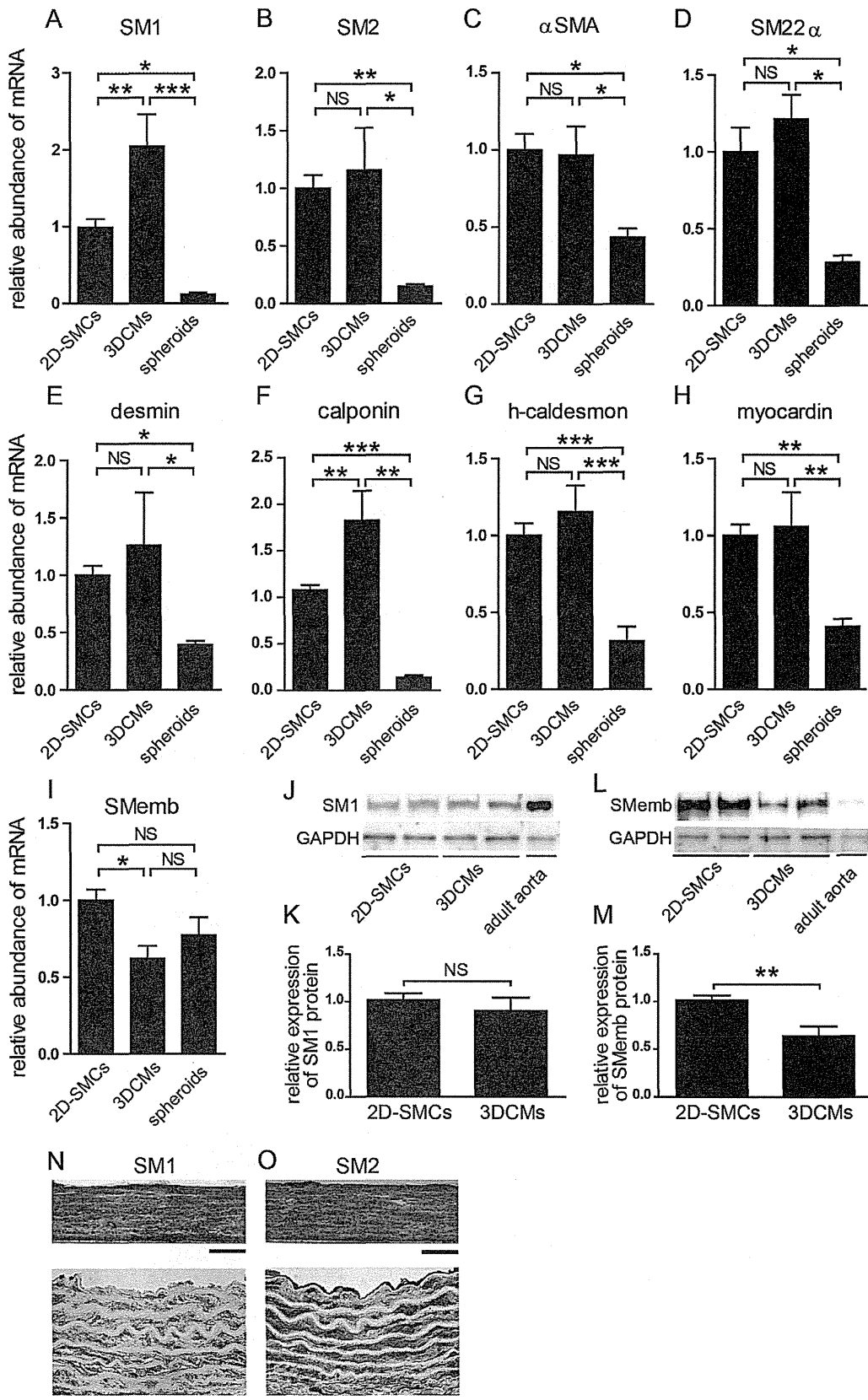


**Fig. 3.** Characterization of SMC phenotype in 3DCMs. (A–H) Messenger RNA expressions of differentiation SMC markers, SM1 (A), SM2 (B), αSMA (C), SM22α (D), desmin (E), calponin (F), h-caldesmon (G), myocardin (H), and a dedifferentiation SMC marker, SMemb (I) in 2D-SMCs, 3DCMs, and SMC spheroids.  $n = 4–8$ . (J) Immunoblot analysis for SM1 in 2D-SMCs and 3DCMs. Rat adult aorta was used as positive control. (K) Quantification of (J).  $n = 10$ . (L) Immunoblot analysis for SMemb in 2D-SMCs and 3DCMs. (M) Quantification of (L).  $n = 10$ . \*,  $p < 0.05$ ; \*\*,  $p < 0.01$ ; \*\*\*,  $p < 0.001$ . NS: not significant. Immunohistochemistry for SM1 (N) and SM2 (O). Brown color indicates positive staining, top panels: 3DCMs. Scale bars: 10 μm lower panels: rat adult aorta. Scale bars: 50 μm.



SMC differentiation in this culture system in comparison to 2D-SMCs and SMC spheroids by monitoring the expression of various SMC markers.

It has been reported that the expression levels of differentiation SMC markers, such as SM1, SM2,  $\alpha$ SMA, SM22 $\alpha$ , and desmin, were highly expressed in the medial layer of SMCs but reduced in human subendothelial intima of atherosclerotic lesions [30–33] and human and rabbit aortic aneurysmal lesions [34,35]. Differentiation SMC markers such as the high molecular weight isoform of caldesmon (h-caldesmon) and calcium-binding protein calponin are also suggested to be downregulated in human atheromatous intima [31,32]. The serum response factor coactivator gene myocardin is required for the expression of many SMC differentiation marker genes and for the initial differentiation of SMC [29]. SMemb is known to be a dedifferentiation SMC marker that is abundantly expressed in human fetal arteries and immature adult cells that are present in vascular injury-induced intima [29]. Expression analysis of mRNAs demonstrated that most differentiation markers were similarly expressed between 2D-SMCs and 3DCMs (Fig. 3A–H). Although the expression levels of SM1 mRNA were higher in 3DCMs than in 2D-SMCs, the SM1 protein expression did not differ between these two culture systems (Fig. 3J–K). Among the SMC phenotypic markers examined, only SMemb was reduced in the 3DCMs compared to the 2D-SMCs in both mRNA and protein (Fig. 3I, L, M).

We also examined the SMC phenotypes of SMC spheroids in comparison with 3DCMs. mRNA expressions of all differentiation SMC markers examined in the whole spheroids were lower than in 3DCMs and even 2D-SMCs (Fig. 3A–H). The expression level of SMemb mRNA in the spheroids was similar to 2D-SMCs and 3DCMs.

Immunohistochemistry showed that SM1 and SM2 proteins were homogeneously expressed in 3DCMs (Fig. 3N, O). In SMC spheroids, SM1 and SM2 were expressed mainly in the outer shell, while the dedifferentiation marker SMemb was expressed in the porous core (Supplemental Fig. 5D, F).

These data suggested that the 3DCMs exhibited similar SMC phenotypes to 2D-SMCs, although a differentiated phenotype was maintained compared to the other types of 3D culture, i.e., SMC spheroids.

#### 3.4. Pharmacological manipulation of elastic fiber formation in 3DCMs

To examine the molecular mechanisms of the elastogenesis and degradation of elastic fibers, and to explore new therapeutic strategies against elastic fiber formation disorders, pharmacological manipulations of 3DCMs are essential. In this context, we examined whether elastic fiber formation in 3DCMs was regulated by the drug that inhibits the cross-linking of elastin monomers to form insoluble elastic fibers [1,26]. When BAPN, an inhibitor of LOX, was applied to 3DCMs for the last two days of culture, the elastic fiber formation was significantly inhibited (Fig. 4A–C).

The biosynthesis of PGE<sub>2</sub> is increased in human atherosclerotic plaques [36] and has been implicated in atherosclerotic plaque rupture [37]. PGE<sub>2</sub> is abundantly produced in aortic aneurysmal lesions and it decreases elastic fiber formation [38,39]. Therefore, we stimulated the 3DCMs with PGE<sub>2</sub> and found that PGE<sub>2</sub> stimulation induced a partial disruption of the layer structure of SMCs (Fig. 4D–E) and decreased elastic fiber formation (Fig. 4F–K). These

data suggest the potential use of 3DCMs for pharmacological manipulation of elastic fiber formation.

#### 3.5. Infiltration of macrophages decreased elastic fibers in 3DCMs

The infiltration of macrophages into the vascular wall is a critical step in the progression of atherosclerosis and aortic aneurysm, and macrophages are the main source of PGE<sub>2</sub>. We applied THP-1 (human monocyte cell line) to the 3DCMs with or without PMA, which induces the differentiation of THP-1, into activated macrophages. Non-activated THP-1 (CTRL) did not infiltrate 3DCMs or affect the SMC layer structure or elastic fiber formation (Fig. 5A, C, E, and G). On the other hand, activated macrophages infiltrated the 3DCMs (Fig. 5D, H) and decreased the surrounding elastic fibers and disrupted the layer structure of SMCs (Fig. 5)B, F, H, and I.

## 4. Discussion

Despite numerous discoveries related to the molecular mechanisms of elastic fiber formation, circulatory diseases associated with elastic fiber disorder, such as aneurysms and atherosclerosis, remain the predominant cause of mortality and morbidity in the developed world [40]. No pharmacological strategy to restore the elastic fiber assembly in diseased vessels or to inhibit the progression of elastin-related diseases is currently available. To obtain further mechanistic insights into elastic fiber formation, in the current study, we sought to create a new experimental vascular model designed specifically for vascular elastic fiber research. We optimized culture conditions and found that 3DCMs consisting of fibronectin-gelatin-coated neonatal rat aortic SMCs cultured in 1% FBS/DMEM exhibited layered elastic fiber formation within seven days, and that the amount of newly synthesized insoluble elastic fibers was significantly greater in 3DCMs than in 2D-SMCs cultured in the same medium.

Recent advances in tissue-engineered blood vessels that are free of synthetic scaffolds enabled the assembly of multiple layers of SMCs and the production of elastic fiber deposition *in vitro* [41]. These techniques provide excellent mechanical properties as implantable vascular constructs but require an excessively long culturing time and/or an *in vivo* bioreactor, neither of which are practical for *ex vivo* experimental vascular models. In this study, fibronectin nanofilms prepared on the surface of SMCs, which has not been used in other tissue-engineered blood vessels, were adopted in 3DCMs for hierarchical cell manipulation and rapid induction of elastic fiber formation. The recent proteomics approach enabled comprehensive molecular interactions in elastic fiber assembly and revealed that fibronectin and microfibrillar fibrillin play a central role [42]. Kinsey et al. and Sabatier et al. demonstrated that, in addition to expression, fibronectin assembly is a prerequisite for fibrillin assembly [10,16]. It is noted that fibronectin assembly and subsequent fibrillin assembly *in vitro* were observed within a couple of days in the static culture condition [10,16]. Other lines of *in vitro* studies demonstrated that fibronectin is critical for the deposition of latent transforming growth factor  $\beta$ -binding protein-1 (LTBP-1), which is associated with microfibrils [11], and that fibronectin assembly promotes LOX activation [14]. Our previous report demonstrated that pericellular fibronectin fibers were observed in 3DCMs within 24 h [9]. In addition, our results demonstrated that the use of  $\epsilon$ -poly(lysine) instead of fibronectin failed to generate elastic fiber formation. These data support our

1 mm. (F–G) EVG stain of 3DCMs. (H–I) Immunofluorescent images of fibrillin-1 in 3DCMs red; fibrillin-1. Scale bars: 50  $\mu$ m. CTRL (D, F, H) and PGE<sub>2</sub> stimulation (E, G, I). (J) top panel: Histograms showing the density of EVG positive area/total area. lower panels: EVG stain of CTRL 3DCMs and PGE<sub>2</sub> stimulated 3DCMs. Scale bars: 100  $\mu$ m. (K) Quantification of density of fibrillin-1 in (H) and (I).  $n = 11$ . \* $p < 0.05$ .

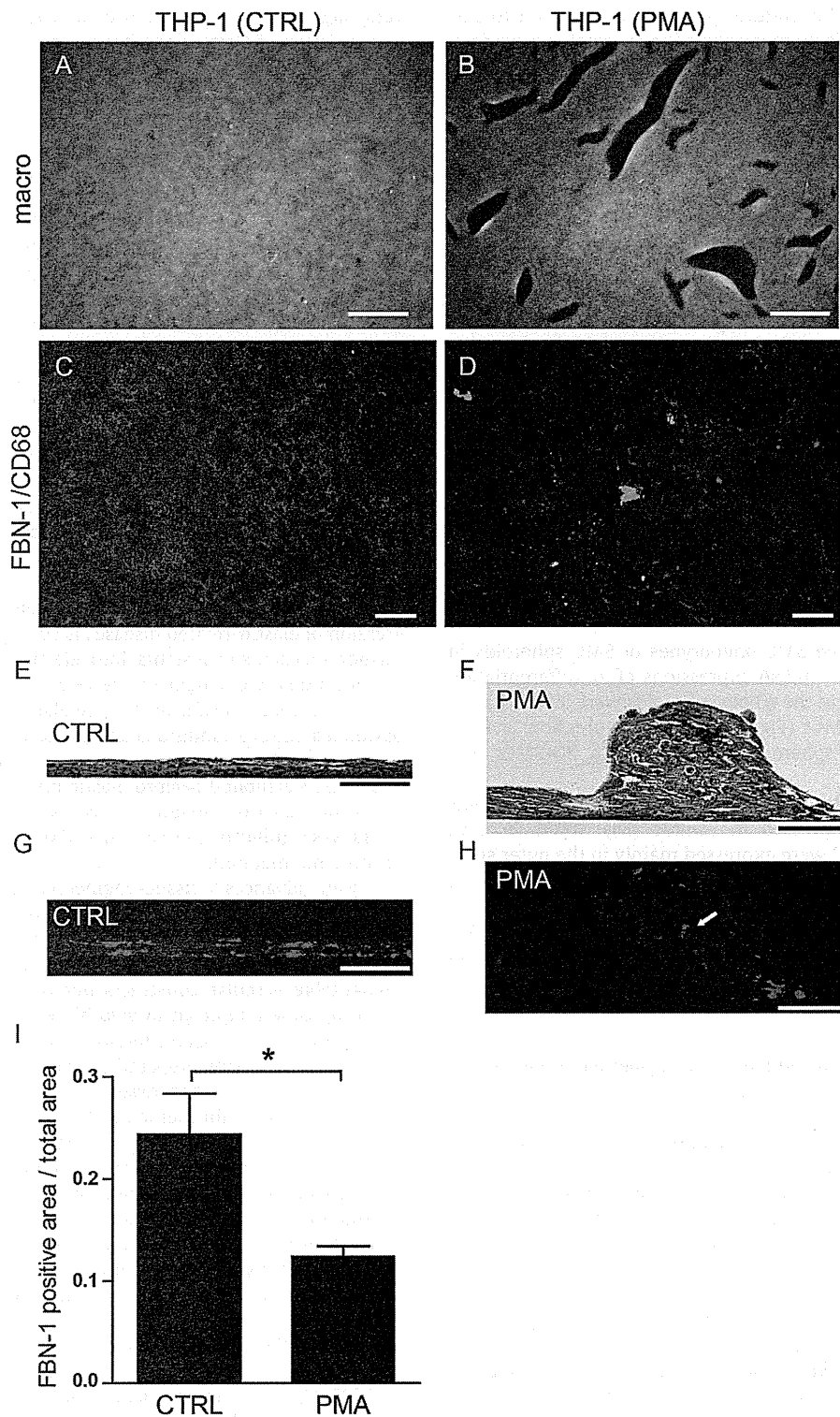


**Fig. 5.** Infiltration of macrophages decreased elastic fibers in 3DCMs (A–B) Macroscopic images of 3DCMs treated with non-activated THP-1 (CTRL), or activated macrophages (PMA). Scale bars: 1 mm. (C–D) Immunofluorescent images of fibrillin-1 (red) and CD68 (green) in 3DCMs. (E–F) EVG stain of 3DCMs. (G–H) Immunofluorescent image of fibrillin-1 (red) and CD 68 (green) in 3DCMs. White arrow indicates infiltrated macrophage. Scale bars: 50  $\mu$ m. (I) Quantification of the density of fibrillin-1 in (G) and (H).  $n = 11$ . \* $p < 0.05$ .

concept that the pericellular fibronectin meshwork on SMCs contributes to elastic fiber assembly in 3DCMs.

Elastin molecules play a crucial role in elastic fiber formation [1]. It has been reported that elastin is expressed maximally at the  $G_0$

and minimally at the  $G_2/M$  phase during the cell cycle [43,44]. In accordance with previous reports, serum withdrawal increased tropoelastin mRNA expression in both 3DCMs and 2D-SMCs. Our data suggest that serum withdrawal–induced cell cycle regulation

has a favorable effect on elastic fiber formation. Fibrillin-2 which contributes to the initial assembly of elastic fibers as well as fibrillin-1 was also induced by serum-starved conditions in both 3DCMs and 2D-SMCs. Cell cycle regulation potentially contributes to the formation of elastic fibers in 3DCMs via the increase in elastin and fibrillin-2.

In addition to the fibronectin nanofilm and culture media component, the use of neonatal vascular SMCs may also contribute to elastic fiber formation in 3DCMs, because it has been well documented that adult vascular SMCs lose the ability to produce components related to elastic fiber assembly, including tropoelastin and fibrillins [1,22,24]. In our study, 3DCMs using adult human aortic SMCs did not produce elastic fibers, even if the same fibronectin coating and culture conditions were applied. In addition to these factors, our data suggest that a certain number of SMC layers are required for elastic fiber formation. Although the exact mechanisms of the rapid induction of elastic fibers in 3DCMs are not known, the multiple factors in 3DCMs, such as the type of SMC, the ECM coated on the cells, the culture media components, and the number of SMC layers are considered to allow layered elastic fibers even in short periods in a static culture condition.

Under physiological conditions, the majority of SMCs in the medial layer of the artery are considered to be in a differentiated (contractile) state that is hardly retained in planar cell culture [29]. Unexpectedly, our results suggest that SMC phenotypes in 3DCMs are similar to those in 2D-SMCs except SMemb expression. Since the differentiated status in SMCs varies through developmental stages and under pathological conditions, including atherosclerosis and vascular injury [45], an understanding of the differentiation status of SMCs in 3DCMs is important in vascular biology research. One study limitation is that SMCs in 3DCMs were not fully differentiated and the elasticity seemed significantly low compared to native vascular tissues. Further modification of 3DCMs, such as modulating SMC phenotypes before creating 3D construction by means of pharmacological stimuli or mechanical stress, is required in future studies.

In the present study, we demonstrated that elastic fiber formation in 3DCMs was disturbed by a LOX inhibitor and PGE<sub>2</sub>, suggesting that pharmacological manipulation could be applied in 3DCMs. The relatively small reduction in elastic fiber formation by BAPN may be due to the 2-day administration out of the 7 days of culture. In conventional *in vivo* study using systemic drug administration, drug metabolism profoundly affects its efficacy, and its indirect effects cannot be discriminated. Although emerging evidence has demonstrated advances in drug delivery systems such as nanoparticles and antibody-drug conjugates that enable tissue-specific targeting strategy, they remain impractical for initial drug screening [46]. 3DCMs may offer a new strategy to examine the direct effects of various drugs on vascular elastic fiber formation and phenotypic changes of SMCs.

There have been excellent *in vitro* systems using 2D culture to examine molecular mechanisms of elastic fiber formation [5–7], because insoluble mature elastic fibers can be formed in certain conditions of 2D culture systems. However, elastic fiber formation in a vertical sectional view cannot be observed in 2D culture systems. In this study, it is suggested that the infiltration of macrophages and its effects on the spatial arrangement of elastic fibers can be observed in 3DCMs.

Spheroid culture system has been established as a 3D culture of SMCs. For example, the spheroids with vascular SMCs retain electrophysiological and contractile properties [47,48]. Paracrine effects of SMCs on gap junction formation of endothelial cells were also shown using the spheroids with human vascular cells [49]. To the best of our knowledge, however, elastic fiber formation and the effect of macrophage infiltration on SMCs have not been reported in

SMC spheroids. Our study revealed that, in SMC spheroids, a few numbers of elastic laminae were formed between the outer shell and porous core at least under the same culture conditions as 3DCMs. Since a single spheroid has around 100  $\mu\text{m}$  in diameter and consists of heterogeneous SMC phenotypes (Supplemental Fig. 5), it seems difficult to construct larger numbers of elastic laminae. On the other hand, the 3DCMs exhibited multiple layered elastic laminae spread over an area of at least 5  $\text{mm}^2$  (Fig. 4D). Furthermore, it was visible with a low magnification that macrophage infiltration induced disruption of elastic fiber assembly in the 3DCMs. In comparison with spheroid culture system, 3DCMs would be suitable for studies of elastic fiber formation in pathophysiological setting.

In conclusion, 3DCMs have the potential to be a new vascular experimental platform in which the spatial and temporal regulation of vascular elastic fibers can be observed. Since the regulation of vascular elastic fiber formation can be examined in 3DCMs, they may be useful for exploring pharmacological therapeutic strategies against disordered elastic fiber homeostasis, such as atherosclerotic vascular disease for which no pharmacological treatment is currently available.

#### Funding sources

This work was supported by grants from the Ministry of Education, Culture, Sports, Science and Technology of Japan (U.Y., Y. Ichikawa, S.M., Y. Ishikawa.), the Grant-in-Aid for Scientific Research on Innovative Areas (UY, 1123116514; Y. Ishikawa, 22136009), the Ministry of Health, Labour and Welfare (Y. Ishikawa), the Grant-in-Aid for Scientific Research (S) from the Japan Society for the Promotion of Science (JSPS)(M.A.), the NEXT Program from JSPS (M.M., LR026) the National Cerebral and Cardiovascular Center (Y. Ishikawa), the Yokohama Foundation for Advanced Medical Science (U.Y.), the Vehicle Racing Commemorative Foundation (U.Y., S.M.), and the Takeda Science Foundation (U.Y., S.M.).

#### Disclosures

No disclosure.

#### Acknowledgments

We are grateful to Yuka Sawada for the excellent technical assistance.

#### Appendix A. Supplementary data

Supplementary data related to this article can be found at <http://dx.doi.org/10.1016/j.atherosclerosis.2014.01.045>.

#### References

- [1] Wagenseil JE, Mecham RP. Vascular extracellular matrix and arterial mechanics. *Physiol Rev* 2009;89:957–89.
- [2] Cheng KS, Baker CR, Hamilton G, et al. Arterial elastic properties and cardiovascular risk/event. *Eur J Vasc Endovasc Surg* 2002;24:383–97.
- [3] Liu C, Zheng D, Zhao L, et al. Elastic properties of peripheral arteries in heart failure patients in comparison with normal subjects. *J Physiol Sci* 2013;63:195–201.
- [4] Nakamura T, Ruiz-Lozano P, Lindner V, et al. DANCE, a novel secreted RGD protein expressed in developing, atherosclerotic, and balloon-injured arteries. *J Biol Chem* 1999;274:22476–83.
- [5] Yeo GC, Baldock C, Tuukkanen A, et al. Tropoelastin bridge region positions the cell-interactive C terminus and contributes to elastic fiber assembly. *Proc Natl Acad Sci U S A* 2012;109:2878–83.

- [6] Wachi H, Sato F, Murata H, et al. Development of a new in vitro model of elastic fiber assembly in human pigmented epithelial cells. *Clin Biochem* 2005;38:643–53.
- [7] Faris B, Jackson LE, Schreiber BM, et al. A controlled precursor add-back model of elastogenesis in smooth muscle cell cultures. *Matrix* 1991;11:367–72.
- [8] Matsusaki M, Kadowaki K, Nakahara Y, et al. Fabrication of cellular multilayers with nanometer-sized extracellular matrix films. *Angew Chem Int Ed Engl* 2007;46:4689–92.
- [9] Matsusaki M, Kadowaki K, Adachi E, et al. Morphological and histological evaluations of 3D-layered blood vessel constructs prepared by hierarchical cell manipulation. *J Biomater Sci Polym Ed* 2012;23:63–79.
- [10] Kinsey R, Williamson MR, Chaudhry S, et al. Fibrillin-1 microfibril deposition is dependent on fibronectin assembly. *J Cell Sci* 2008;121:2696–704.
- [11] Dallas SL, Sivakumar P, Jones CJ, et al. Fibronectin regulates latent transforming growth factor-beta (TGF beta) by controlling matrix assembly of latent TGF beta-binding protein-1. *J Biol Chem* 2005;280:18871–80.
- [12] Sottile J, Shi F, Rublyevska I, et al. Fibronectin-dependent collagen I deposition modulates the cell response to fibronectin. *Am J Physiol Cell Physiol* 2007;293:C1934–46.
- [13] Velling T, Risteli J, Wennerberg K, et al. Polymerization of type I and III collagens is dependent on fibronectin and enhanced by integrins alpha 11beta 1 and alpha 2beta 1. *J Biol Chem* 2002;277:37377–81.
- [14] Fogelgren B, Polgar N, Szauter KM, et al. Cellular fibronectin binds to lysyl oxidase with high affinity and is critical for its proteolytic activation. *J Biol Chem* 2005;280:24690–7.
- [15] Wierzbicka-Patynowski I, Schwarzbauer JE. The ins and outs of fibronectin matrix assembly. *J Cell Sci* 2003;116:3269–76.
- [16] Sabatier L, Chen D, Fagotto-Kaufmann C, et al. Fibrillin assembly requires fibronectin. *Mol Biol Cell* 2009;20:846–58.
- [17] Yokoyama U, Minamisawa S, Quan H, et al. Chronic activation of the prostaglandin receptor EP4 promotes hyaluronan-mediated neointimal formation in the ductus arteriosus. *J Clin Invest* 2006;116:3026–34.
- [18] Yokoyama U, Minamisawa S, Adachi-Akahane S, et al. Multiple transcripts of Ca<sup>2+</sup> channel alpha 1-subunits and a novel spliced variant of the alpha1C-subunit in rat ductus arteriosus. *Am J Physiol Heart Circ Physiol* 2006;290:H1660–70.
- [19] Jin MH, Yokoyama U, Sato Y, et al. DNA microarray profiling identified a new role of growth hormone in vascular remodeling of rat ductus arteriosus. *J Physiol Sci* 2011;61:167–79.
- [20] Hirai M, Ohbayashi T, Horiguchi M, et al. Fibulin-5/DANCE has an elastogenic organizer activity that is abrogated by proteolytic cleavage in vivo. *J Cell Biol* 2007;176:1061–71.
- [21] Yokoyama U, Minamisawa S, Shioda A, et al. Prostaglandin E2 inhibits elastogenesis in the ductus arteriosus via EP4 signaling. *Circulation* 2013;129:487–96.
- [22] Kelleher CM, McLean SE, Mecham RP. Vascular extracellular matrix and aortic development. *Curr Top Dev Biol* 2004;62:153–88.
- [23] Wagenseil JE, Mecham RP. New insights into elastic fiber assembly. *Birth Defects Res C Embryo Today* 2007;81:229–40.
- [24] McMahon MP, Faris B, Wolfe BL, et al. Aging effects on the elastin composition in the extracellular matrix of cultured rat aortic smooth muscle cells. *Vitro Cell Dev Biol* 1985;21:674–80.
- [25] Long JL, Tranquillo RT. Elastic fiber production in cardiovascular tissue-equivalents. *Matrix Biol* 2003;22:339–50.
- [26] Kagan HM, Li W. Lysyl oxidase: properties, specificity, and biological roles inside and outside of the cell. *J Cell Biochem* 2003;88:660–72.
- [27] Hirai M, Horiguchi M, Ohbayashi T, et al. Latent TGF-beta-binding protein 2 binds to DANCE/fibulin-5 and regulates elastic fiber assembly. *EMBO J* 2007;26:3283–95.
- [28] Horiguchi M, Inoue T, Ohbayashi T, et al. Fibulin-4 conducts proper elastogenesis via interaction with cross-linking enzyme lysyl oxidase. *Proc Natl Acad Sci U S A* 2009;106:19029–34.
- [29] Owens GK, Kumar MS, Wamhoff BR. Molecular regulation of vascular smooth muscle cell differentiation in development and disease. *Physiol Rev* 2004;84:767–801.
- [30] Aikawa M, Sivam PN, Kuro-o M, et al. Human smooth muscle myosin heavy chain isoforms as molecular markers for vascular development and atherosclerosis. *Circ Res* 1993;73:1000–12.
- [31] Glukhova MA, Kabakov AE, Frid MG, et al. Modulation of human aorta smooth muscle cell phenotype: a study of muscle-specific variants of vinculin, caldesmon, and actin expression. *Proc Natl Acad Sci U S A* 1988;85:9542–6.
- [32] Shanahan CM, Cary NR, Metcalfe JC, et al. High expression of genes for calcification-regulating proteins in human atherosclerotic plaques. *J Clin Invest* 1994;93:2393–402.
- [33] Kocher O, Gabbiani G. Cytoskeletal features of normal and atheromatous human arterial smooth muscle cells. *Hum Pathol* 1986;17:875–80.
- [34] Kamijima T, Isobe M, Suzuki J, et al. Enhanced embryonic nonmuscle myosin heavy chain isoform and matrix metalloproteinase expression in aortic abdominal aneurysm with rapid progression. *Cardiovasc Pathol* 1999;8:291–5.
- [35] Jiao L, Xu Z, Xu F, et al. Vascular smooth muscle cell remodeling in elastase-induced aortic aneurysm. *Acta Cardiol* 2010;65:499–506.
- [36] Cipollone F, Fazio ML, Iezzi A, et al. Association between prostaglandin E receptor subtype EP4 overexpression and unstable phenotype in atherosclerotic plaques in human. *Arterioscler Thromb Vasc Biol* 2005;25:1925–31.
- [37] Linton MF, Fazio S. Cyclooxygenase products and atherosclerosis. *Drug Discov Today Ther Strateg* 2008;5:25–36.
- [38] Walton LJ, Franklin IJ, Bayston T, et al. Inhibition of prostaglandin E2 synthesis in abdominal aortic aneurysms: implications for smooth muscle cell viability, inflammatory processes, and the expansion of abdominal aortic aneurysms. *Circulation* 1999;100:48–54.
- [39] Yokoyama U, Ishiwata R, Jin MH, et al. Inhibition of EP4 signaling attenuates aortic aneurysm formation. *PLoS One* 2012;7:e36724.
- [40] Lloyd-Jones D, Adams RJ, Brown TM, et al. Heart disease and stroke statistics—2010 update: a report from the American Heart Association. *Circulation* 2010;121:e46–215.
- [41] Peck M, Gebhart D, Dusserre N, et al. The evolution of vascular tissue engineering and current state of the art. *Cells Tissues Organs* 2012;195:144–58.
- [42] Cain SA, McGovern A, Small E, et al. Defining elastic fiber interactions by molecular fishing: an affinity purification and mass spectrometry approach. *Mol Cell Proteomics* 2009;8:2715–32.
- [43] Wachi H, Seyama Y, Yamashita S, et al. Cell cycle-dependent regulation of elastin gene in cultured chick vascular smooth-muscle cells. *Biochem J* 1995;309(Pt 2):575–9.
- [44] Seyama Y, Wachi H. Atherosclerosis and matrix dystrophy. *J Atheroscler Thromb* 2004;11:236–45.
- [45] Aikawa M, Yamaguchi H, Yazaki Y, et al. Smooth muscle phenotypes in developing and atherosclerotic human arteries demonstrated by myosin expression. *J Atheroscler Thromb* 1995;2:14–23.
- [46] Lobatto ME, Fuster V, Fayad ZA, et al. Perspectives and opportunities for nanomedicine in the management of atherosclerosis. *Nat Rev Drug Discov* 2011;10:835–52.
- [47] Gentile C, Fleming PA, Mironov V, et al. VEGF-mediated fusion in the generation of uniluminal vascular spheroids. *Dev Dyn* 2008;237:2918–25.
- [48] Harder DR, Sperelakis N. Action potential generation in reagggregates of rat aortic smooth muscle cells in primary culture. *Blood Vessels* 1979;16:186–201.
- [49] Korff T, Kimmina S, Martiny-Baron G, et al. Blood vessel maturation in a 3-dimensional spheroidal coculture model: direct contact with smooth muscle cells regulates endothelial cell quiescence and abrogates VEGF responsiveness. *FASEB J* 2001;15:447–57.

# Store-Operated $\text{Ca}^{2+}$ Entry (SOCE) Regulates Melanoma Proliferation and Cell Migration

Masanari Umemura<sup>1\*</sup>, Erdene Baljinnyam<sup>2</sup>, Stefan Feske<sup>3</sup>, Mariana S. De Lorenzo<sup>2</sup>, Lai-Hua Xie<sup>2</sup>, Xianfeng Feng<sup>1</sup>, Kayoko Oda<sup>1</sup>, Ayako Makino<sup>1</sup>, Takayuki Fujita<sup>1</sup>, Utako Yokoyama<sup>1</sup>, Mizuka Iwatsubo<sup>2</sup>, Suzie Chen<sup>4</sup>, James S. Goydos<sup>5</sup>, Yoshihiro Ishikawa<sup>1</sup>, Kousaku Iwatsubo<sup>1,2\*</sup>

**1** Cardiovascular Research Institute, Yokohama City University School of Medicine, Yokohama, Japan, **2** Department of Cell Biology and Molecular Medicine, New Jersey Medical School, Rutgers, The State University of New Jersey, Newark, New Jersey, United States of America, **3** Department of Pathology, New York University School of Medicine, New York, New York, United States of America, **4** Department of Chemical Biology, Susan Lehman Cullen Laboratory of Cancer Research in the Ernest Mario School of Pharmacy, Rutgers, The State University of New Jersey, Piscataway, New Jersey, United States of America, **5** Division of Surgical Oncology, Department of Surgery, Robert Wood Johnson Medical School, Rutgers, The State University of New Jersey, Piscataway, New Jersey, United States of America

## Abstract

Store-operated  $\text{Ca}^{2+}$  entry (SOCE) is a major mechanism of  $\text{Ca}^{2+}$  import from extracellular to intracellular space, involving detection of  $\text{Ca}^{2+}$  store depletion in endoplasmic reticulum (ER) by stromal interaction molecule (STIM) proteins, which then translocate to plasma membrane and activate Orai  $\text{Ca}^{2+}$  channels there. We found that STIM1 and Orai1 isoforms were abundantly expressed in human melanoma tissues and multiple melanoma/melanocyte cell lines. We confirmed that these cell lines exhibited SOCE, which was inhibited by knockdown of STIM1 or Orai1, or by a pharmacological SOCE inhibitor. Inhibition of SOCE suppressed melanoma cell proliferation and migration/metastasis. Induction of SOCE was associated with activation of extracellular-signal-regulated kinase (ERK), and was inhibited by inhibitors of calmodulin kinase II (CaMKII) or Raf-1, suggesting that SOCE-mediated cellular functions are controlled via the CaMKII/Raf-1/ERK signaling pathway. Our findings indicate that SOCE contributes to melanoma progression, and therefore may be a new potential target for treatment of melanoma, irrespective of whether or not Braf mutation is present.

**Citation:** Umemura M, Baljinnyam E, Feske S, De Lorenzo MS, Xie L-H, et al. (2014) Store-Operated  $\text{Ca}^{2+}$  Entry (SOCE) Regulates Melanoma Proliferation and Cell Migration. PLoS ONE 9(2): e89292. doi:10.1371/journal.pone.0089292

**Editor:** Laszlo Csernoch, University of Debrecen, Hungary

**Received:** May 29, 2013; **Accepted:** January 21, 2014; **Published:** February 21, 2014

**Copyright:** © 2014 Umemura et al. This is an open-access article distributed under the terms of the Creative Commons Attribution License, which permits unrestricted use, distribution, and reproduction in any medium, provided the original author and source are credited.

**Funding:** This study was supported by the American Heart Association (SDG 0835596D) and by the Foundation of UMDNJ and by the Melanoma Research Foundation (K. Iwatsubo). This study was also supported by the Japan Heart Foundation and by the Kanagawa Nanbyo Foundation (M. Umemura). This study was supported in part by the Ministry of Health, Labor and Welfare, a Grant-in-Aid for Scientific Research on Innovative Areas (22136009), and the Japanese Ministry of Education, Culture, Sports, Science, and Technology (Y. Ishikawa). The funders had no role in study design, data collection and analysis, decision to publish, or preparation of the manuscript.

**Competing Interests:** The authors have declared that no competing interests exist.

\* E-mail: iwatuko@njms.rutgers.edu (KI); umemurma@yokohama-cu.ac.jp (MU)

## Introduction

Melanoma has the poorest prognosis among skin cancers, although drugs targeting aberrant ERK signaling, i.e., mutated serine/threonine-protein kinase Braf, have improved both overall and progression-free survival times [1]. However, this therapy is not effective in patients without Braf mutation, and some patients with Braf mutation rapidly acquire resistance to Braf inhibitors [2]. Accordingly, a different approach to target ERK signaling regardless of Braf mutation is needed.

Intracellular  $\text{Ca}^{2+}$  signaling regulates diverse cellular functions including proliferation and cell migration [3]. Store-operated  $\text{Ca}^{2+}$  entry (SOCE) is a major mechanism of  $\text{Ca}^{2+}$  import from extracellular to intracellular space, especially in non-excitable cells [4]. In general, activation of inositol 1,4,5-trisphosphate ( $\text{IP}_3$ ) receptors on the endoplasmic reticulum (ER) evokes a rapid and transient release of  $\text{Ca}^{2+}$  from the ER store. The resulting decrease of  $\text{Ca}^{2+}$  concentration in the ER is sensed by the EF-hand motif of stromal interaction molecules (STIM), which then translocate to the plasma membrane, where they interact with Orai  $\text{Ca}^{2+}$  channel subunits [5], leading to  $\text{Ca}^{2+}$  influx from extracellular space to restore the  $\text{Ca}^{2+}$  concentration in ER [6].

The physiological functions of STIM and Orai have been studied mainly in connection with the immune system [7–10]. Orai channels control  $\text{Ca}^{2+}$  release-activated  $\text{Ca}^{2+}$  (CRAC) currents in lymphocytes [4], and also contribute to SOCE currents in other types of cells, such as endothelial cells [11]. STIM1 and Orai1, but not STIM2, Orai2 or Orai3, have roles in cell migration of smooth muscle cells [12,13]. Examination of a library of randomized ribozymes indicated that STIM1 is a metastasis-related gene [14]. SOCE is involved in proliferation, cell migration, and angiogenesis in cervical cancer [15], and cell migration in breast cancer [16]. However, the role of SOCE in melanoma has been little investigated, except for a recent paper demonstrating Akt signaling activation in mouse melanoma cells, especially in lipid rafts [17]. In the present study, we show that SOCE promotes melanoma progression by enhancing cell proliferation, migration, and metastasis through activation of ERK signaling via the CaMKII/Raf-1/ERK pathway.

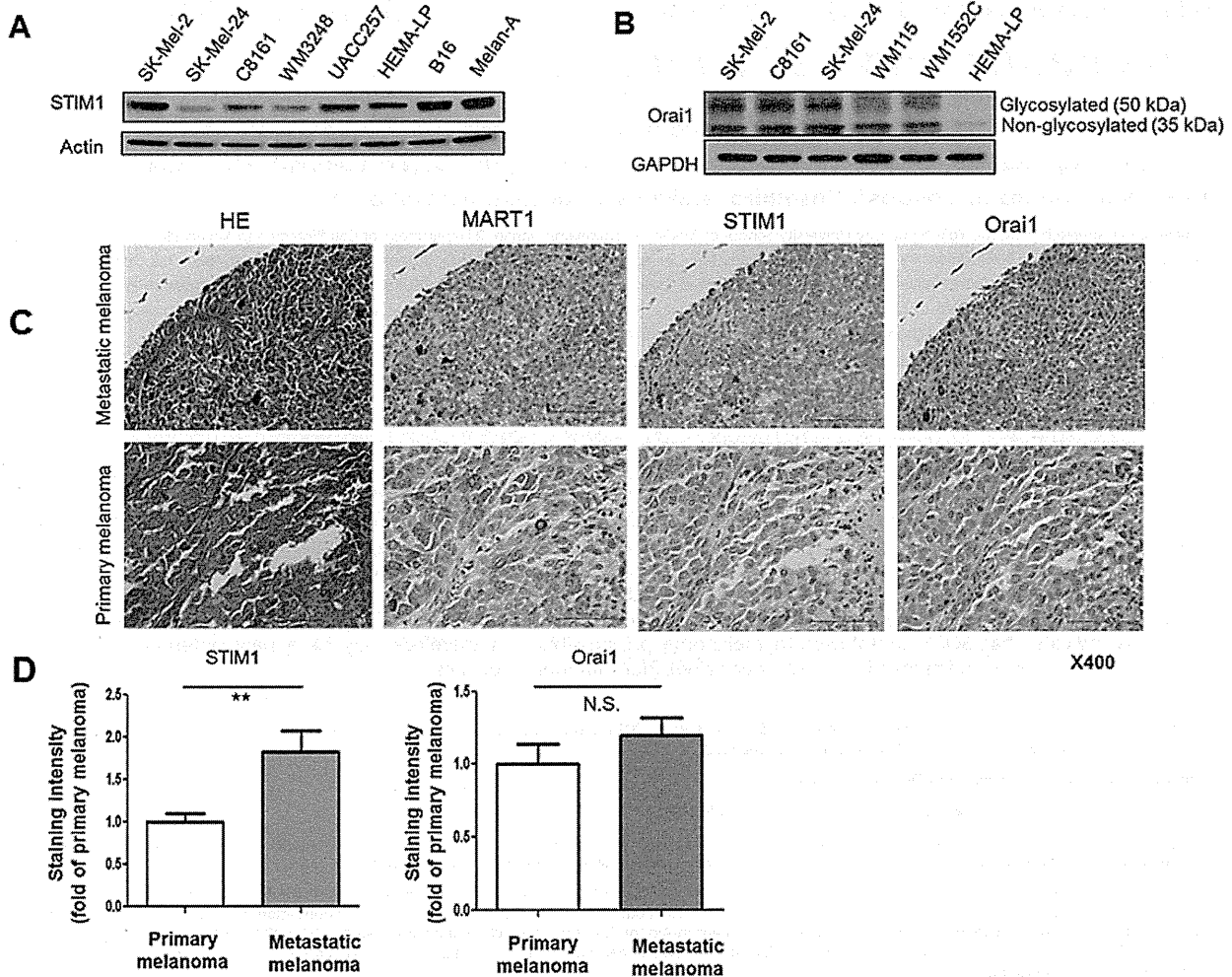


**Figure 1. Expression of STIM1 and Orai1 in melanoma.** (A and B) Western blot analyses of STIM1 (A) and Orai1 (B) expression in the indicated cell lines. (C) Immunohistochemical stainings of HE, MART1, STIM1 (the antibody from Abnova was used) and Orai1 (the antibody from Sigma was used) in a melanoma tissue microarray (original magnification, x400). Calibration bars represent 100  $\mu$ m. (D) Analyses of the staining intensity of expression of STIM1 and Orai1. \*,  $p < 0.05$ ; \*\*,  $p < 0.01$ ,  $n = 8$ . doi:10.1371/journal.pone.0089292.g001

## Materials and Methods

### Reagents and Cell Lines

Reagents were purchased from Sigma unless otherwise specified. Antibodies to  $\beta$ -actin, GAPDH, and ERK were purchased from Santa Cruz.  $\alpha$ -Spectrin antibody was purchased from Millipore. Phospho-ERK antibody was purchased from Cell Signaling. Antibodies against STIM1 were purchased from BD Transduction Laboratories and Abnova [18]. Antibodies against Orai1 were previously generated by us [19], or purchased from Sigma [12]. Second antibodies for mouse and rabbit were purchased from Abcam and Cell Signaling, respectively. GW5074 was purchased from Focus Biomolecules. W5 hydrochloride was purchased from Tokyo Chemical Industry. GDC-0879 was purchased from Selleckchem [20]. SK-Mel-2 and SK-Mel-24 (human metastatic melanoma) cell lines were obtained from the American Type Culture Collection. UACC257 (human metastatic melanoma) was obtained from the Charles River Laboratory. Melan-A mouse melanocyte cell line was purchased from Wellcome Trust Functional Genomics Cell Bank, St.

George's, University of London. C8161 cell line was kindly provided by Dr. Mary J.C. Hendrix. WM3248 and WM115 (primary melanoma, vertical growth phase (VGP)) and WM1552C (primary melanoma, radial growth phase (RGP)) cell lines were kindly provided by Dr. Meenhard Herlyn. HEMA-LP (human melanocyte) cell line was obtained from Invitrogen. SK-Mel-2 and SK-Mel-24 cells were maintained in MEM containing 10% fetal bovine serum (FBS) and 1% penicillin-streptomycin. UACC257 cells were maintained in RPMI-1640 (Sigma) containing 10% FBS and 1% penicillin-streptomycin. HEMA-LP was maintained in an EndoGRO-VEGF Complete media kit (Millipore). All other melanoma cells were maintained in RPMI (Gibco) containing 10% FBS and 1% penicillin-streptomycin.

### Western Blot Analysis

Western blot analyses were performed as we previously described [21]. Briefly, cells were lysed and sonicated in RIPA buffer (Thermo Scientific). Equal amounts of protein were subjected to sodium dodecyl sulfate polyacrylamide gel electro-

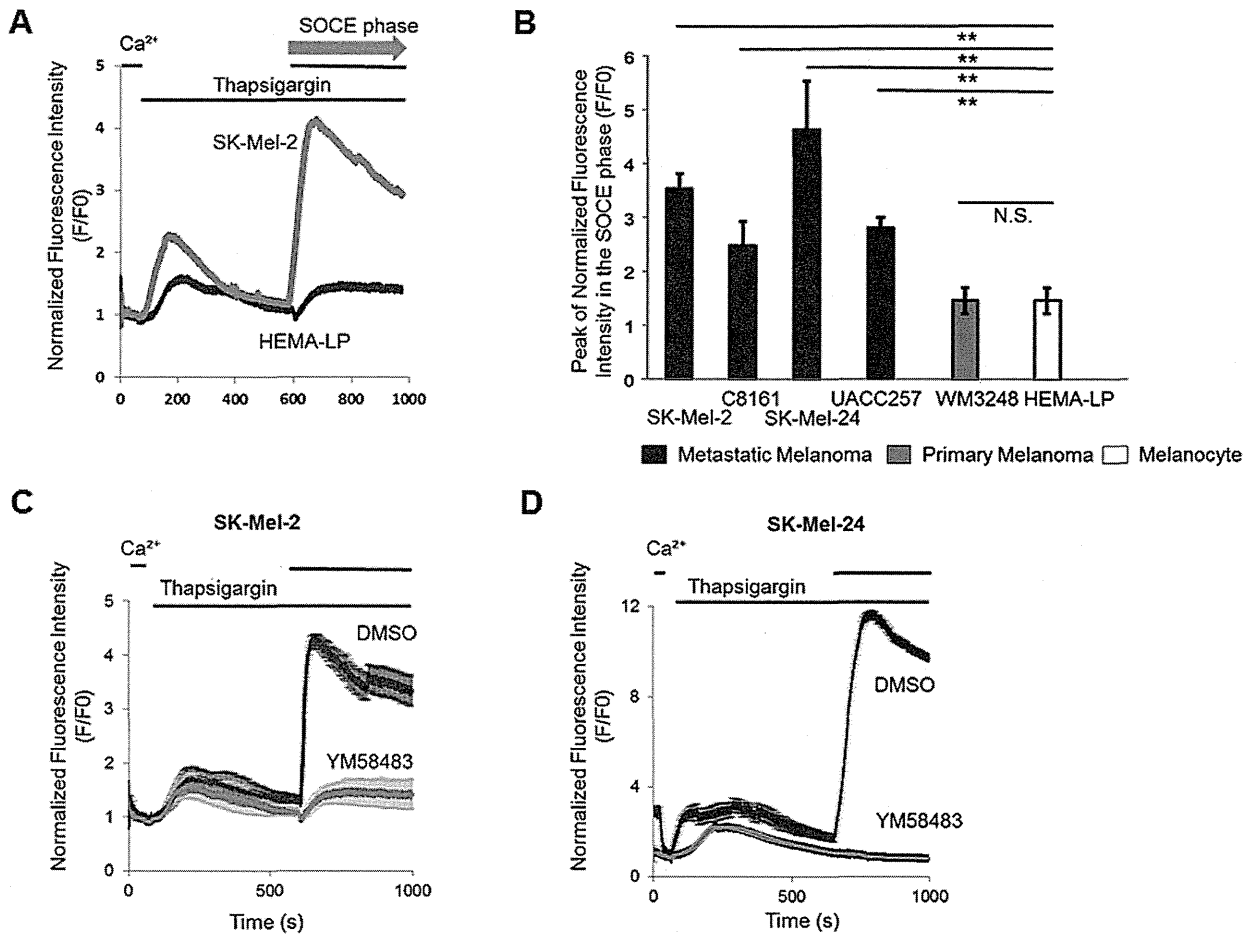


**Figure 2. SOCE occurs in melanoma.** (A) Cytosolic  $\text{Ca}^{2+}$  levels in SK-Mel-2 cells. Extracellular  $\text{Ca}^{2+}$  (2 mM) was removed, followed by the addition of thapsigargin (TG) (2  $\mu\text{M}$ ) for  $\text{Ca}^{2+}$  depletion in the ER.  $\text{Ca}^{2+}$  (2 mM) was then added to the extracellular fluid, and SOCE-induced  $\text{Ca}^{2+}$  elevation was observed (SOCE phase). (B)  $\text{Ca}^{2+}$  peak amplitude in the SOCE phase was compared among melanoma and melanocyte cell lines. \*\*,  $p < 0.01$  (HEMA-LP),  $n = 6-8$ . (C and D) Cytosolic  $\text{Ca}^{2+}$  levels in SK-Mel-2 and SK-Mel-24 cells are shown as means  $\pm$  SD ( $n = 6-10$ ). SOCE was examined in the presence or absence of DMSO (1  $\mu\text{M}$ ) or YM58483 (1  $\mu\text{M}$ ) in SK-Mel-2 (C) and SK-Mel-24 cells (D). doi:10.1371/journal.pone.0089292.g002

phoresis (SDS-PAGE). After protein separation by electrophoresis, samples were transferred to Millipore Immobilon-P membrane followed by immunoblotting with antibodies against molecules of interest. Immunoblottings for STIM1 and Orai1 were performed with the antibodies from BD Transduction Laboratories and from Sigma, respectively. Signal intensities of bands were quantified with Image J software (NIH).

### Immunohistochemistry

Immunohistochemical stainings were performed as we previously described [22]. Melanoma tissue microarray plates (US Biomax Cat. #T085 and #ME1004a) were subjected to immunohistochemistry with antibodies against melanoma antigen recognized by T-cells 1 (MART1) (Millipore), STIM1 and Orai1. Two different antibodies against STIM1 (purchased from BD Transduction Laboratories and Abnova) and Orai1 (generated by us [19] and purchased from Sigma) were used to confirm the specificity of the staining. Negative control samples were exposed to the secondary antibody alone. Quantification of STIM1 expression was performed with BZ-II analyzer software (Keyence) as we previously described [23].

### Fluorescence Imaging of Intracellular $\text{Ca}^{2+}$

Measurement of intracellular  $\text{Ca}^{2+}$  level was performed as we previously described [24]. Cells were incubated with 2-[4-(2-hydroxyethyl)-1-piperazinyl]ethanesulfonic acid (HEPES) buffer containing 4  $\mu\text{mol/l}$  of Fluo-4AM, followed by washing and incubation with HEPES-buffered saline containing 2.0 mmol/L of  $\text{CaCl}_2$ . An iXon+885 charge-coupled-device camera (Andor Technology) was used to monitor fluorescence changes. Full images were collected every 4 s. Fluo-4 fluorescence was excited at 488 nm, and data were expressed as normalized changes in background-corrected fluorescence emission ( $F/F_0$ ). Data were analyzed using Imaging Workbench (INDEC BioSystems). Representative  $\text{Ca}^{2+}$  signals averaged from 6 to 10 individual cells are shown in the figures.

### Transduction of Short Hairpin RNA (shRNA)

SK-Mel-2, SK-Mel-24 and C8161 cells were transduced with STIM1 shRNA, Orai1 shRNA, and scramble control shRNA using lentivirus (Santa Cruz Biotechnology) according to the protocols provided by the manufacturer. Briefly, cells were incubated with 10  $\mu\text{g/mL}$  of Polybrene (Santa Cruz Biotechnol-

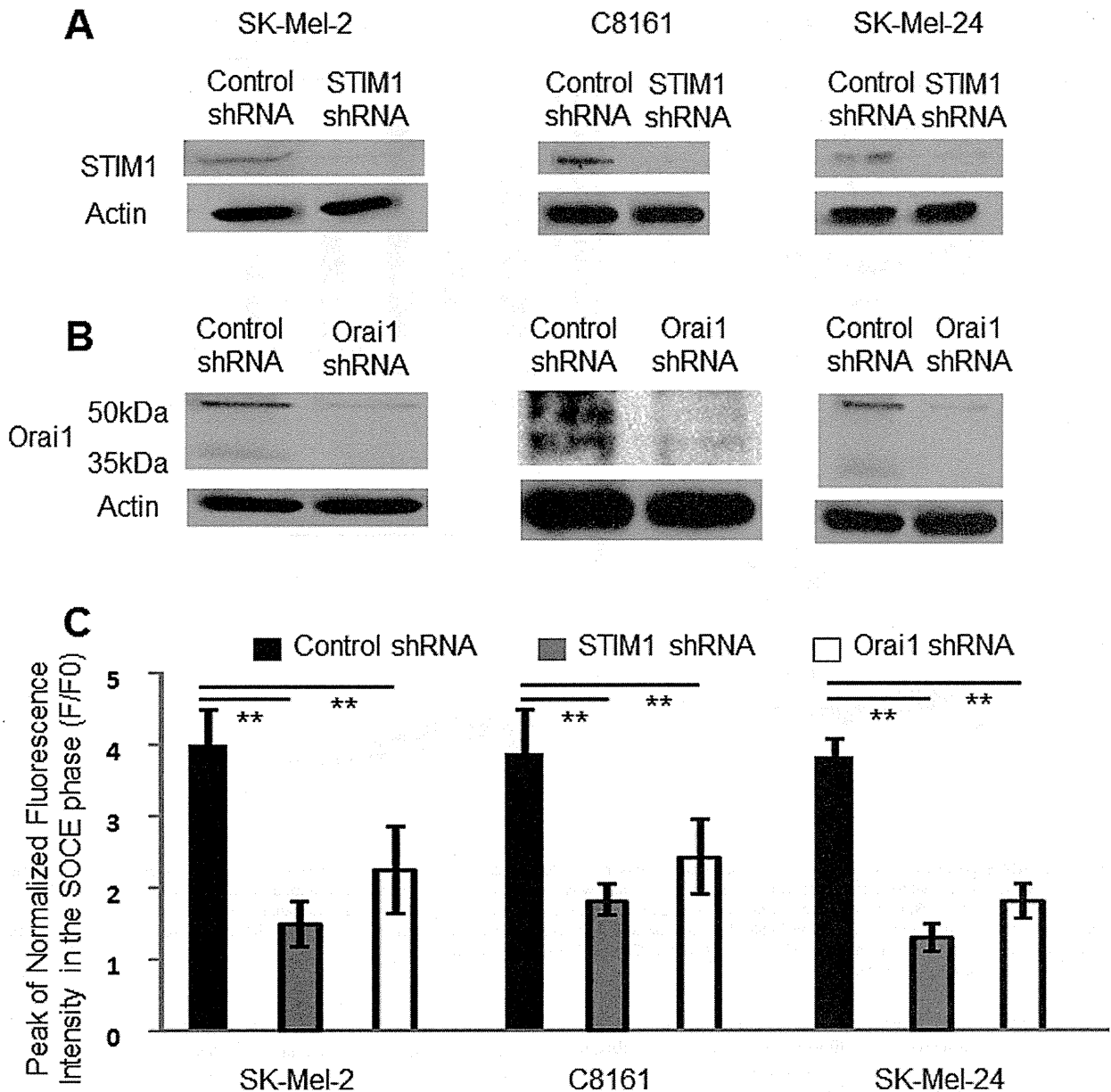


**Figure 3. SOCE was inhibited by STIM1- or by Orai1-knockdown in melanoma cell lines.** (A and B) Western blot analyses of protein expressions of STIM1 (A) and Orai1 (B) in metastatic melanoma cell lines. shRNA transduction reduced expression of the target proteins. (C)  $Ca^{2+}$  peak amplitude of SOCE was reduced by STIM1- or Orai1-knockdown. \*\*,  $p < 0.01$ ,  $n = 6-10$ . doi:10.1371/journal.pone.0089292.g003

ogy) and lentiviral particles harboring each shRNA, then selected with puromycin dihydrochloride (Santa Cruz Biotechnology) for 1 week. Puromycin-containing medium was replaced with fresh medium every 3 to 4 days.

#### 3-(4,5-Dimethylthiazol-2-yl)-2,5-diphenyltetrazolium Bromide (MTT) Assay

Cells were seeded in a 96-well plate at 5,000 or 10,000 cells per well and cultured for 24 h. Viable cells were determined daily using the MTT Cell Proliferation Assay kit (ATCC) according to the manufacturer's instructions.

#### Apoptosis Assays

Apoptosis assays were performed as previously described [25]. Cells were seeded on 6 cm dishes, and incubated for 24 or 48 hours. Cells were washed twice with cold PBS, and transferred into culture tubes. Annexin V, allophycocyanin conjugate (APC) and 7-amino-actinomycin D (7-AAD) (BD Biosciences, California, U.S.A.) were then added to the tubes. Cells were incubated for 15 min at RT (25°C) in darkness, followed by FACS analysis (Canto™ II, Japan Becton, Dickinson and Company, Tokyo, Japan) within 1 hour.

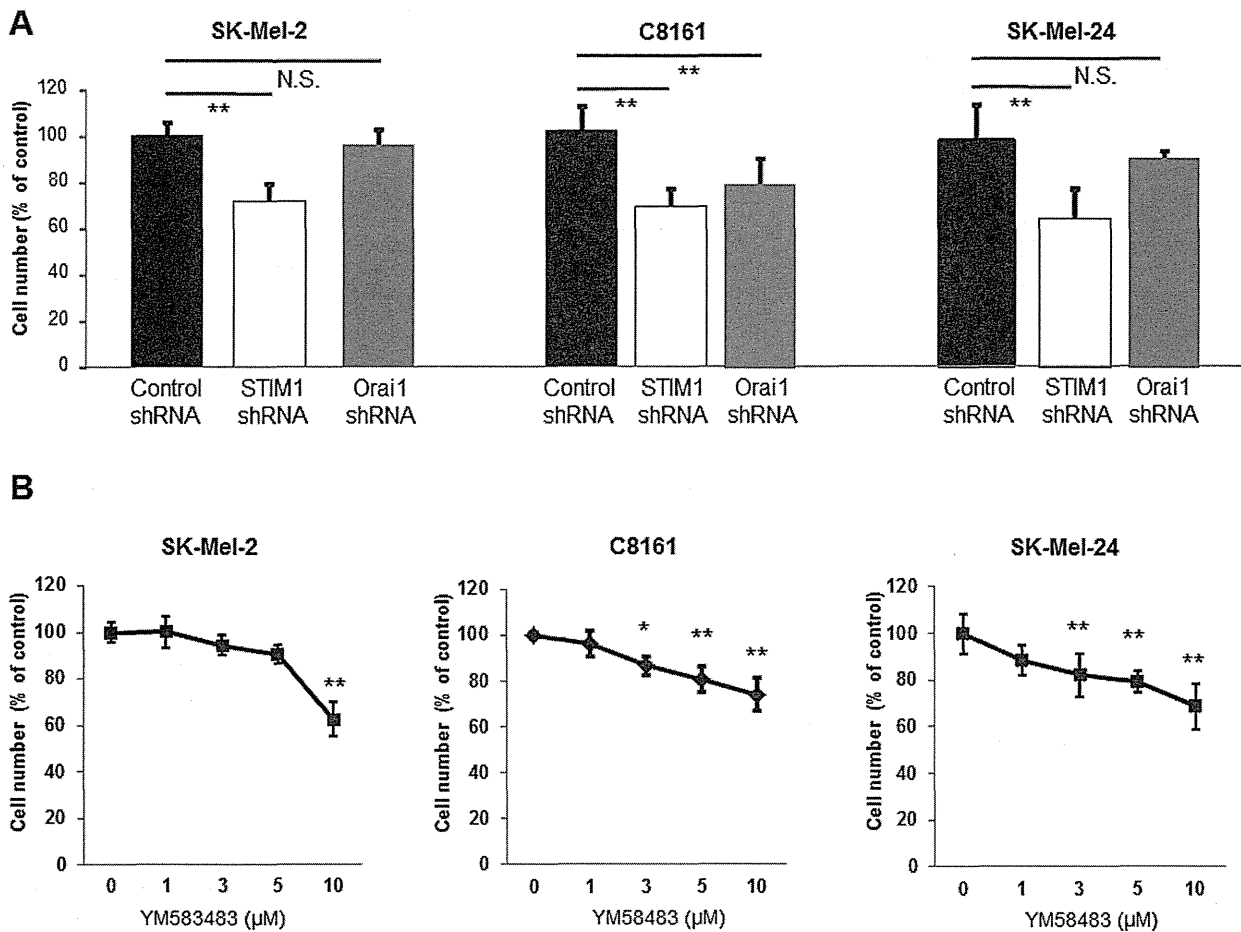


**Figure 4. SOCE regulates proliferation of melanoma cells.** (A) MTT assay of metastatic melanoma cell lines with or without STIM1- or Orai1-knockdown. \*\*,  $p < 0.01$ ,  $n = 8$ . Representative data of 3 independent experiments are shown. (B) MTT assay of the indicated cell lines in the presence or absence of YM58483. \*,  $p < 0.05$ ; \*\*,  $p < 0.01$ ,  $n = 8$ . Representative data of 3 independent experiments are shown. doi:10.1371/journal.pone.0089292.g004

### Migration Assays

Migration assays were performed using 24-well Boyden chambers (8  $\mu\text{m}$  pores, BD Biosciences) as we previously described [25]. The cells were plated at a density of  $1 \times 10^5$  cells/100  $\mu\text{l}$  of medium in the inserts, and incubated for 3 h at 37°C, followed by staining using a Diff-Quick kit (SIMENS). Pictures were taken with a microscope to count the number of migrated cells. The scratch wound method was also employed in some experiments as follows. Cells were seeded and allowed to form a monolayer for 24 h. The dish was scraped with the tip of a 100  $\mu\text{l}$  pipette, and the resulting wound was washed with PBS two times [12]. Culture medium containing 10% FBS was added to the cells, and the cells were incubated at 37°C in 5%  $\text{CO}_2$ . Bright-field images were captured (Olympus IX51 microscope) and analyzed (Adobe Photoshop). The total number of pixels in empty spaces inside the wound were counted and normalized to the control.

### Time-lapse Videomicroscopy

Analysis of cell motility using time-lapse videomicroscopy was performed as we previously described [25]. SK-Mel-2 cells were subjected to time-lapse video recording. Frames from the recording were digitized at 15-min intervals. Moving distance of each cell was analyzed by Image J software (NIH).

### Calpain Activity Assay

Calpain activity was performed as previously described [26] with the calpain activity kit (Abcam) according to the manufacturer's instructions.

### Immunocytochemistry

Immunocytochemistry was performed as previously described [24]. Filamentous actin (F-actin) staining was performed by incubation with rhodamine phalloidin (Invitrogen). Photographs were taken with a digital camera on a Nikon Eclipse TE200, and cells with one lamellipodium or more were counted manually.

### Lung Colonization Assay

Lung colonization assay was performed as we previously described [22]. Cells were harvested and injected ( $2 \times 10^6$  cells/0.2 ml) into the tail veins of BALB/c nude mice (Charles River, male, 8 weeks old). Three weeks after the injection, metastatic colonies on the surface of the lungs were fixed with picric acid and counted under a dissection microscope.

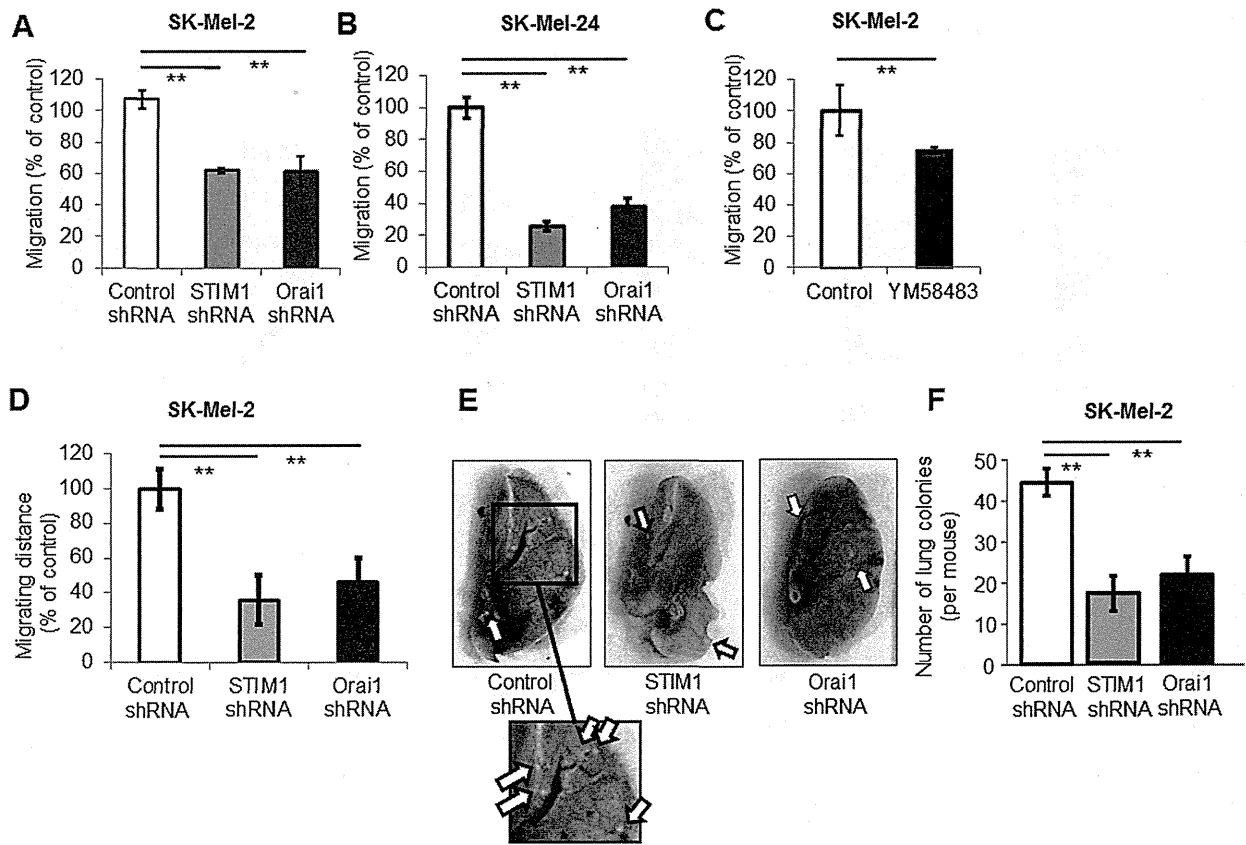


**Figure 5. SOCE regulates cell migration and metastasis of melanoma.** (A and B) Boyden chamber assay showed that either STIM1- or Orai1-knockdown inhibited cell migration. \*\*,  $p < 0.01$ ,  $n = 4$ . (C) The scratch test showed that YM58483 (1  $\mu$ M) inhibited cell migration. \*\*,  $p < 0.01$ ,  $n = 4$ . (D) Time-lapse video recording (Videos S1, S2, and S3) showed that STIM1- or Orai1-knockdown SK-Mel-2 cells exhibited a shorter migration distance than control SK-Mel-2 cells. \*\*,  $p < 0.01$ ,  $n = 10$ . (E and F) SK-Mel-2 cells with knockdown of either STIM1 or Orai1 were injected to the tail vein of Balb/c nu/nu mice. Three weeks later, the lungs were removed and fixed with picric acid. (E) Representative images of lung surface are shown. Arrows indicate metastatic melanoma colonies (white lesions). (F) The number of metastatic colonies in the lung surface was counted under a dissection microscope. \*\*,  $p < 0.01$ ,  $n = 8$ . doi:10.1371/journal.pone.0089292.g005

#### Data Analysis and Statistics

Statistical comparisons among groups were performed using Student's *t*-test or one-factor analysis of variance (ANOVA) with the Bonferroni post hoc test. The criterion of statistical significance was set at  $p < 0.05$ . \*,  $p < 0.05$ , \*\*,  $p < 0.01$ , N.S., not significant.

#### Ethics Statement

All animal studies were approved by the Institutional Animal Care and Use Committees of New Jersey Medical School-Rutgers, The State University of New Jersey (Protocol Number: 11104D0914).

#### Results

##### STIM1 and Orai1 are Expressed in Human Melanoma

We first examined expression of STIM and Orai in human melanoma. Western blot analyses showed that STIM1 and Orai1 are expressed in metastatic human melanoma cell lines, while the melanocyte cell line, HEMA-LP, displayed only a low level of Orai1 expression (Fig. 1A and B). In contrast, STIM2, Orai2 and Orai3 expression was undetectable or barely detectable in the melanoma cell lines (data not shown). We also examined expression of STIM1 and Orai1 in human melanoma tissues,

using a microarray. Both molecules were immunohistochemically detected (Fig. 1C). Interestingly, STIM1, but not Orai1, showed higher expression in metastatic melanoma than in primary melanoma (Fig. 1D). This finding was confirmed using a different set of antibodies. These data suggested that STIM1 expression, but not Orai1 expression, positively correlates with melanoma progression.

##### SOCE Occurs in Melanoma Cell Lines

Since STIM1 and Orai1 were detected in human melanoma tissues, we examined whether SOCE occurs in melanoma cell lines. SOCE is defined as enhanced  $Ca^{2+}$  import from extracellular space after depletion of  $Ca^{2+}$  stores in the ER. Experimentally, SOCE is induced by  $Ca^{2+}$  addition after  $Ca^{2+}$  depletion from the ER with thapsigargin (Fig. 2A), an inhibitor of sarcoplasmic reticulum  $Ca^{2+}$ -ATPase (SERCA). We observed SOCE in some melanoma and melanocyte cell lines examined (Fig. 2B). Metastatic (SK-Mel-2, C8161, SK-Mel-24 and UACC2577), but not primary (WM3248, WM115 (data not shown) and WM1552C (data not shown)), melanoma cell lines showed higher SOCE peak amplitudes than the melanocyte cell line (HEMA-LP). These data suggested that SOCE is enhanced in metastatic melanoma, in accordance with the idea that activation of SOCE is related to

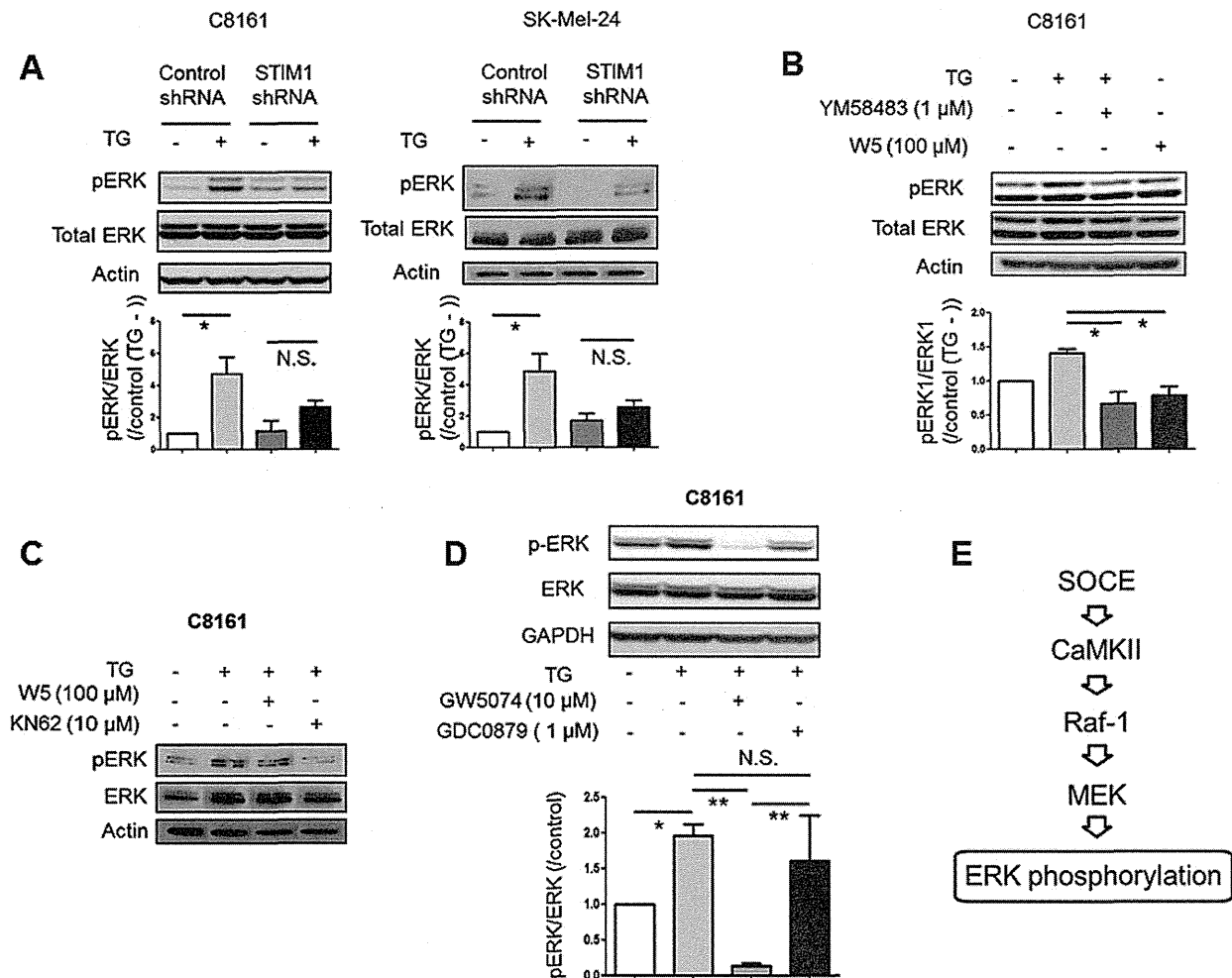


**Figure 6. SOCE increases phosphorylation of ERK in melanoma.** (A) Densitometric analyses (bar graph) of western blots show that thapsigargin increased phosphorylation of ERK1/2 in metastatic melanoma cell lines. STIM1-knockdown inhibited thapsigargin-induced phosphorylation of ERK1/2. \*,  $p < 0.05$ ; N.S., not significant,  $n = 3$ . (B) Densitometric analyses (bar graph) of western blots show that thapsigargin-induced phosphorylation of ERK1/2 was inhibited by SOCE inhibitor YM58483 and CaM inhibitor W5 in C8161 cells. \*,  $p < 0.05$ ,  $n = 3$ . (C) Thapsigargin-induced phosphorylation of ERK1/2 was inhibited by CaM inhibitor W5 and CaMKII inhibitor KN62 in C8161 cells. (D) Densitometric analyses (bar graph) of western blots show that thapsigargin-induced phosphorylation of ERK1/2 was inhibited by Raf-1 inhibitor GW5074, but not by Braf inhibitor GDC0879. \*,  $p < 0.05$ ; \*\*,  $p < 0.01$ ; N.S. not significant,  $n = 3$ . (E) Proposed signaling schema of SOCE-induced ERK activation. doi:10.1371/journal.pone.0089292.g006

melanoma progression. A pyrazole compound, YM58483, which is known to inhibit SOCE in non-melanoma cells [27,28], also suppressed SOCE in metastatic melanoma cell lines (Fig. 2C and D).

#### STIM1- or Orai1-knockdown Inhibits SOCE in Melanoma Cell Lines

We examined whether SOCE in melanoma cell lines is regulated by STIM1 and Orai1.  $Ca^{2+}$  peak amplitude in the SOCE phase was lower in both STIM1- (Fig. 3A) and Orai1- (Fig. 3B) knockdown cells than in control metastatic melanoma cell lines (Fig. 3C). These data suggested that both STIM1 and Orai1 are involved in SOCE activation in melanoma.

#### Inhibition of SOCE Suppresses Melanoma Cell Proliferation

We next examined the role of SOCE in cellular functions of melanoma. We found that proliferation was reduced in STIM1-knockdown metastatic melanoma cell lines (Fig. 4A). This was not due to induction of apoptosis, because there was no significant difference of apoptosis between STIM1-knockdown and control C8161 cells after both 24 hours and 48 hours (Fig. S1). In contrast, Orai1-knockdown inhibited proliferation in C8161 cells but not in SK-Mel-2 or SK-Mel-24 cells, suggesting that STIM1, rather than Orai1, is the key determinant of melanoma proliferation. The SOCE inhibitor YM58483 (Fig. 4B) inhibited proliferation of SK-Mel-2, C8161 and SK-Mel-24 cells, further supporting the view that SOCE plays an important role in melanoma proliferation.

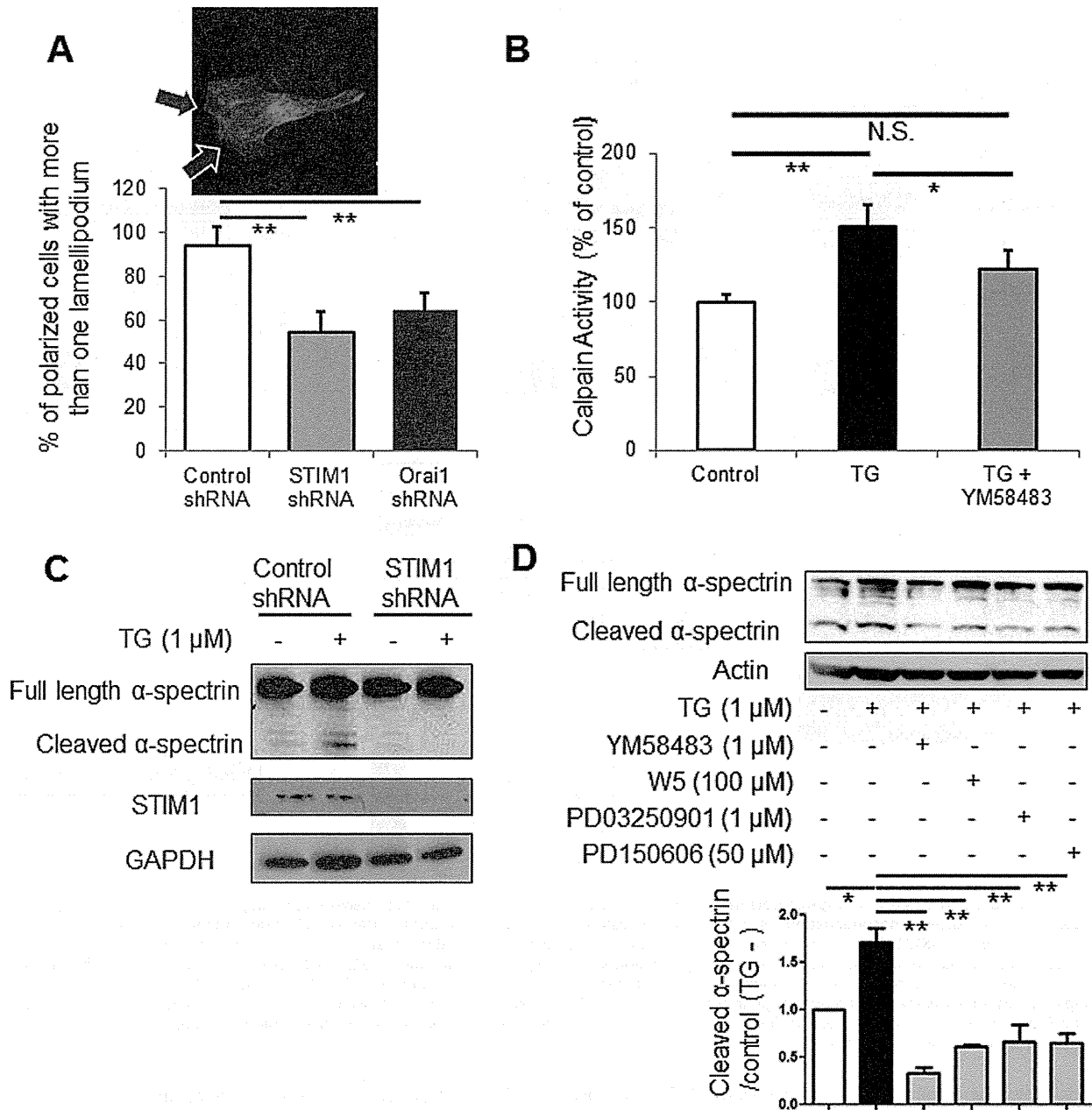


**Figure 7. Proposed mechanisms of SOCE-mediated cellular functions in melanoma.** (A) The upper panel shows actin staining of SK-Mel-2 cells. Arrows indicate lamellipodia. The lower panel shows the number of SK-Mel-2 cells with more than one lamellipodium. \*\*,  $p < 0.01$ ,  $n = 331$  for control shRNA, 850 for STIM1 shRNA, and 986 for Orai1 shRNA. (B) Calpain activity assay shows that thapsigargin increased calpain activity. Thapsigargin-induced elevation of calpain activity was inhibited by YM58483. \*,  $p < 0.05$ , \*\*,  $p < 0.01$ , N.S., not significant,  $n = 4$ . (C) Western blot analyses showed that thapsigargin (TG) increased cleavage of α-spectrin in SK-Mel-2 cells. Thapsigargin-induced cleavage of α-spectrin was inhibited by STIM1-knockdown. Representative data of 3 independent experiments are shown. (D) Densitometric analyses (bar graph) of western blots show that thapsigargin-induced cleavage of α-spectrin was inhibited by SOCE inhibitor YM58483, CaM inhibitor W5, MEK inhibitor PD03250901, and calpain inhibitor PD150606. \*,  $p < 0.05$ ; \*\*,  $p < 0.01$ ,  $n = 3$ . doi:10.1371/journal.pone.0089292.g007

**Inhibition of SOCE Suppresses Melanoma Cell Migration/ Metastasis**

Since  $Ca^{2+}$  signaling regulates migration of cancer cells [29], we also examined the role of SOCE in melanoma cell migration. We found that both STIM1- and Orai1-knockdown inhibited cell

migration in metastatic melanoma cell lines (Fig. 5A and B). YM58483 also inhibited melanoma cell migration (Fig. 5C). Time-lapse video recordings showed reduced cell migration distance of both STIM1- and Orai1-knockdown cells (Fig. 5D and Videos S1, S2, and S3). We next examined whether the reduced cell migration is correlated with inhibition of metastasis. Both STIM1-

and Orail-knockdown resulted in decreased numbers of metastatic colonies in the lungs of mice (Fig. 5E and F). These data suggested that the inhibition of SOCE suppresses melanoma cell migration and thereby reduces metastasis.

### SOCE Regulates ERK Signaling in Melanoma Cell Lines

The ERK signaling pathway is known to play a major role in melanoma cells migration and proliferation [30,31]. Thus, we next examined whether SOCE affects ERK signaling. Phosphorylation of ERK1/2, which reflects activity of ERK signaling, was increased by thapsigargin in metastatic melanoma cell lines (Fig. 6A). The thapsigargin-induced ERK1/2 phosphorylation was attenuated by STIM1-knockdown (Fig. 6A) and by YM58483 (Fig. 6B), suggesting that thapsigargin-induced ERK activation occurs via a SOCE-related mechanism. Since it has been demonstrated that intracellular  $Ca^{2+}$  activates ERK signaling via calmodulin (CaM)/calmodulin-dependent protein kinase II (CaMKII) [32], we examined the involvement of these molecules in the SOCE-induced ERK activation. Thapsigargin-induced ERK1/2 phosphorylation was inhibited by W5, a CaM inhibitor (Fig. 6B and C), and by KN62, a CaMKII inhibitor (Fig. 6C), suggesting that SOCE-induced ERK activation is mediated by CaM/CaMKII. Thapsigargin-induced ERK1/2 phosphorylation was inhibited by GW5074, a specific Raf-1 inhibitor, but not by GDC0879, a specific Braf inhibitor, in C8161 cells (Fig. 6D). This is in accordance with previous findings that CaMKII can bind to and activate Raf-1 [33,34]. Similar results were also observed in SK-Mel-24 cells (data not shown), suggesting that Raf-1, rather than Braf, predominantly mediates SOCE-mediated ERK activation (Fig. 6E). These data suggested that the conventional ERK signaling pathway is activated by SOCE via CaM/CaMKII.

### SOCE Regulates Melanoma Cell Migration via ERK Signaling

There have been extensive studies on the mechanism of melanoma cell proliferation via ERK signaling [35,36]. However, the molecular mechanism through which ERK signaling regulates melanoma cell migration remains relatively unclear. Intracellular  $Ca^{2+}$  accelerates cell migration via calpain, a proteolytic enzyme, which promotes actin assembly/disassembly [37,38]. Therefore, it was suggested that SOCE regulates melanoma cell migration via calpain-dependent actin dynamics. This hypothesis was supported by the observation that the number of lamellipodia, which reflects the activity of actin assembly/disassembly [39,40], was decreased by STIM1- or Orail-knockdown (Fig. 7A). In addition, we found that calpain activity was increased by thapsigargin, but was inhibited by YM58483 (Fig. 7B). Further, cleavage of  $\alpha$ -spectrin, a target enzyme of calpain, was increased by thapsigargin, but was inhibited by STIM1-knockdown (Fig. 7C). These data suggested that SOCE regulates cell migration in a calpain-dependent manner. The question of how SOCE activates calpain then arises. Calpain was originally found as a  $Ca^{2+}$ -dependent enzyme [41], but recently it was demonstrated that ERK signaling can increase calpain activity [42–44]. We thus examined whether ERK signaling rather than intracellular  $Ca^{2+}$  itself modulates calpain activity. As shown in Fig. 7D, thapsigargin-induced  $\alpha$ -spectrin cleavage was inhibited by YM58483, and by PD150606, a calpain inhibitor, as expected. In addition, inhibition of CaM by W5 and inhibition of MEK by PD03250901 suppressed thapsigargin-induced  $\alpha$ -spectrin cleavage. These data suggested that calpain mediates SOCE-induced cell migration via ERK signaling, not via simple SOCE-induced elevation of intracellular  $Ca^{2+}$ .

## Discussion

Our present findings show that SOCE occurs in melanoma cells and plays a pivotal role in cell proliferation and migration, most probably via ERK signaling. STIM1 and Orail were expressed not only in cultured melanoma cells, but also in human melanoma tissues. SOCE activity in melanoma cells was dependent on STIM1 and Orail, and was reduced by SOCE inhibitor YM58483. Inhibition of SOCE suppressed both melanoma proliferation and cell migration. In addition, SOCE activated ERK signaling in melanoma cells, which may lead to further changes in cellular functions. Accordingly, our results suggest that melanoma progression is promoted by SOCE via ERK signaling. Recent melanoma therapies have targeted V600E-mutated Braf [1], but some patients are non-responders, and acquisition of resistance is also a problem [2]. Our data showed that SOCE occurs not only in melanoma cells bearing Braf-mutation (SK-Mel-24, UACC257, WM3248, WM115, and WM1552C), but also in non-Braf-mutation-carrying melanoma cell lines (SK-Mel-2 and C8161). In addition, we found that STIM1-knockdown inhibited ERK phosphorylation in both Braf-mutated (SK-Mel-24) and non-Braf-mutated (SK-Mel-2 and C8161) cells. These data suggested that inhibition of SOCE suppresses ERK signaling activity irrespective of the existence of Braf mutation. Therefore, targeting SOCE could potentially benefit a greater number of melanoma patients, compared to currently used Braf inhibitors.

The role of SOCE in proliferation and cell migration is well established. Abdullaev *et al.* showed that STIM1 and Orail regulate CRAC currents and SOCE, leading to changes in proliferation of endothelial cells [11]. In vascular smooth muscle cells, knockdown of either STIM1 or Orail, but not of STIM2, Orail2, and Orail3, inhibited proliferation and cell migration [13]. In cancer cells, Yang *et al.* reported that STIM1-knockdown inhibited serum-induced breast tumor cell migration [16]. The same group also showed that STIM1-knockdown in hepatocarcinoma cells affects disassembly and turnover of focal adhesion [45]. Our data demonstrate that STIM1 and Orail have roles in proliferation and migration of various melanoma cell lines, indicating that SOCE contributes to melanoma progression. Orail knockdown had only a minor effect on proliferation compared to STIM1 knockdown, suggesting that TRPC channels rather than Orail potentially interact with STIM1 [46] in the regulation of proliferation. There was a discrepancy between the effective concentrations of YM58483 for inhibition of proliferation and inhibition of SOCE. This can be attributed, at least in part, to compensatory upregulation of SOCE [47], which would occur during the relatively prolonged exposure to the SOCE-inhibitory drug in MTT assay compared to the short exposure during SOCE measurement. Another concern is the fact that Orail deletion did not inhibit proliferation of SK-Mel-2 and SK-Mel-24 cells, whereas YM58483 treatment did. This might be explained by incomplete knockdown of Orail.

It was recently demonstrated that, in mouse melanoma cells, SOCE occurs in lipid rafts, and ablation of the rafts suppressed tumor growth, most probably via the Akt pathway [48]. These data, taken together with ours, indicate that SOCE regulates multiple pathways in melanoma, supporting our proposal that SOCE plays a pivotal role in melanoma progression.

The upstream pathway leading to SOCE in melanoma cells remains unknown.  $Ca^{2+}$  depletion in the ER is mainly controlled by the phospholipase C (PLC)/IP<sub>3</sub>/IP<sub>3</sub> receptor pathway, which is generally activated by either tyrosine kinase-type receptors or Gq-related G protein coupled receptors. Previous reports indicated that SOCE is controlled by tyrosine kinase-type receptors rather